ADVANCED OPTICAL MATERIALS
www.advopticalmat.de

Recent Progress in Mixed A-Site Cation Halide Perovskite Thin-Films and Nanocrystals for Solar Cells and Light-Emitting Diodes

Mahdi Malekshahi Byranvand, Clara Otero-Martínez, Junzhi Ye, Weiwei Zuo, Liberato Manna, Michael Saliba,* Robert L. Z. Hoye,* and Lakshminarayana Polavarapu**

Over the past few years, lead-halide perovskites (LHPs), both in the form of bulk thin films and colloidal nanocrystals (NCs), have revolutionized the field of optoelectronics, emerging at the forefront of next-generation optoelectronics. The power conversion efficiency (PCE) of halide perovskite solar cells has increased from 3.8% to over 25.7% over a short period of time and is very close to the theoretical limit (33.7%). At the same time, the external quantum efficiency (EQE) of perovskite LEDs has surpassed 23% and 20% for green and red emitters, respectively. Despite great progress in device efficiencies, the photoactive phase instability of perovskites is one of the major concerns for the long-term stability of the devices and is limiting their transition to commercialization. In this regard, researchers have found that the phase stability of LHPs and the reproducibility of the device performance can be improved by A-site cation alloying with two or more species, these are named mixed cation (double, triple, or quadruple) perovskites. This review provides a state-of-the-art overview of different types of mixed A-site cation bulk perovskite thin films and colloidal NCs reported in the literature, along with a discussion of their synthesis, properties, and progress in solar cells and LEDs.

1. Introduction

Metal-halide perovskites have attracted enormous interest for optoelectronic applications, such as solar cells,[1–3] light-emitting diodes (LEDs),[4–6] lasers,[7] photodetectors,[8] and radiation detectors[9] due to their exceptional properties, such as high absorption coefficients (>10^5 cm^{-1}), tunable bandgaps, long charge-carrier diffusion lengths, and low exciton binding energies.[10–14] Perovskite solar cells (PSCs) have shown unprecedented rises in power conversion efficiency (PCE) from 3.8%[3] in 2009 to a certified value of 25.7% in 2022[15–17] by optimizing the composition,[1,18] crystallization,[19] and interfaces of perovskite films.[16,20] This remarkable rise in PCE puts PSCs at the forefront of emerging PVs, including dye-sensitized solar cells (DSCs),[21] organic photovoltaics (OPVs),[22,23] and quantum dot solar

M. M. Byranvand, W. Zuo, M. Saliba
Institute for Photovoltaics (ipv)
University of Stuttgart
Pfaffenwaldring 47, 70569 Stuttgart, Germany
E-mail: michael.saliba@ipv.uni-stuttgart.de

M. M. Byranvand, M. Saliba
Helmholtz Young Investigator Group FRONTRUNNER
IEK5-Photovoltaik
Forschungszentrum Jülich
52425 Jülich, Germany

C. Otero-Martínez, L. Polavarapu
CINBIO
Universidade de Vigo
Materials Chemistry and Physics Group
Department of Physical Chemistry
Campus Universitario As Lagoas – Marcosende, Vigo 36310, Spain
E-mail: lakshmi@uvigo.es

The ORCID identification number(s) for the author(s) of this article can be found under https://doi.org/10.1002/adom.202200423.

DOI: 10.1002/adom.202200423

J. Ye
Cavendish Laboratory
University of Cambridge
19, JJ Thomson Avenue, Cambridge CB3 0HE, UK

L. Manna
Nanochemistry Department
Istituto Italiano di Tecnologia
Genova 16163, Italy
E-mail: liberato.manna@iit.it

R. L. Z. Hoye
Department of Materials
Imperial College London
Exhibition Road, London SW7 2AZ, UK
E-mail: r.hoye@imperial.ac.uk

cells.[24] These low-temperature processed PSCs have performance that are comparable to the best crystalline silicon solar cells.[25] Moreover, the tunable bandgap of perovskite materials (1.2 to 3.0 eV) provides the opportunity to use them as both the top and bottom cells in tandem structures, overcoming the Shockley–Queisser efficiency limit of 33.7% for single-junction solar cells.[26–28] Generally, metal halide perovskites are described with the ABX_3 formula, where the A-site is an organic (typically $CH_3NH_3^+$ (MA^+) and $NH_2CHNH_2^+$ (FA^+)) or inorganic cation (typically Cs^+, Rb^+, K^+),[29,30] the B-site is a metal cation (typically Pb^{2+} or Sn^{2+}),[31,32] and X is a halide (typically, Cl^-, Br^-, or I^-).[33,34] In structurally 3D perovskites, the central metal cation is octahedrally coordinated with 6 halides, that is, $[BX_6]^{4-}$. The A-site cations fill the cuboctahedral voids to compensate for the negative charge of $[BX_6]^{4-}$ and stabilize the perovskite lattice. Depending on the number of A-site cations in the crystal lattice, they can be differentiated into mono, double, triple, and quadruple A-cation perovskites. The most common A-cations that can fit into cuboctahedral voids of the perovskite structure are MA, FA, and Cs, while the position of small cations (such as K, Na, and Rb) and the large cations (such as methylenediammonium (MDA) cations) is being debated. Therefore, herein we named them dopants, and they can either occupy the A-site vacancies or interstitial sites. The possibility of forming different perovskite crystal structures and their phase stability can be predicted by the Goldschmidt tolerance factor (GTF), defined as $t = (r_A + r_X)/\sqrt{2}(r_B + r_X)$, where r_A, r_B, and r_X are the ionic radius of ions in A, B, and X sites, respectively.[35] Generally, it has been empirically found that when the GTFs are in the range of $0.8 < \text{GTF} < 1.0$, the perovskite structure presents a stable crystallographic phase (see **Figure 1**b).[36,37] The size of A-site cations in the perovskite structure is crucial for determining the crystallographic phase that forms. For example, A-site cations with smaller (Na^+, K^+, Rb^+, or Cs^+) or larger sizes (FA^+) than ideal cations lead to GTFs lower than 0.8 or higher than 1.0 values, resulting in the 3D-symmetric structure with corner-sharing octahedra transitioning to hexagonal non-perovskite phases with edge or face-sharing octahedra (Figure 1b).[36–38] Although the GTF has been successfully used to predict the phase stability of various perovskite compositions, there are still many exceptions that cannot be entirely interpreted by this empirical formula, and there have been efforts to define refined versions that are accurate in predicting which compositions give rise to perovskite structures.[37–39]

The inorganic octahedral metal-halide framework, that is, $[BX_6]^{4-}$, is responsible for the optoelectronic properties of perovskites. As shown in the energy level diagram of the halide perovskite (Figure 1c), the 6s orbitals of Pb^{2+} hybridize with the outer p orbitals (3p, 4p, and 5p for Cl, Br, and I, respectively) of the halide, leading to bonding and antibonding states that form in the valence band, while the empty 6p orbitals of Pb^{2+} hybridize with outer p orbitals of the halide to form bonding states within the valence band and an antibonding state in the conduction band minimum.[40] A slightly different energy level picture has also been proposed, in which the outer s electrons of halides also interact p and s orbitals of Pb, leading to an s orbital contribution in the conduction band.[14,41] The A-site cation in the perovskite structure typically directly affects the intrinsic and extrinsic stabilities, as well as physiochemical properties. However, in lead-halide perovskites (LHPs), the bonding with the A-site cation is ionic, such that the inorganic or organic cation does not contribute states to the band-edges. As shown in Figure 1d, these states are dominated by the hybridization of the B-site and X-site orbitals, which have more covalent interactions. These species therefore more directly influence the bandgap and optoelectronic properties of the halide perovskites.[42] That being said, the A-site cation can also play an indirect role in the band structure by influencing the bond lengths, and thus bandgap, and angles between the B- and X-site species, such as through octahedral tilting of the inorganic sub-lattice, or through steric interactions.[43] The bandgap slightly decreases with increasing the size of the A-cation from Cs to MA to FA due to decreased tilting angle of PbX—Pb bonds. Therefore, the properties of the A-site cation, including their size, shape, and charge distribution, can change the electronic structure of perovskites near the band edges.[41] For example, FA^+ is, from a thermodynamic perspective, too large to fit into the cuboctahedral voids at room temperature, leading to non-photoactive phases with an unfavorable bandgap for photovoltaic applications (Figure 1b). However, mixing cations with different sizes and shapes into the A-site can stabilize the stable black photoactive phase at room temperature by altering the GTF.[44] For instance, the reduction in GTF obtained by partially substituting FA^+ in $FAPb(I/Br)_3$ with a smaller cation (MA^+ or Cs^+) compensates for the increase in GTF caused by the replacement of I with Br.[45] In this regard, combinatorial libraries for perovskite materials were introduced to facilitate effective compositional engineering and high-throughput screening of novel metal–halide perovskite materials.[46] In principle, the number of the possible combinations can be deduced from the well-known Pascal triangle, using $\sum_{k}^{n}\binom{n}{k} = 2^n$, referring to possibility to choose a subset of k elements from an overall set with n elements. Various single, double, triple, and quadruple formulations at the A-site could be achieved based on different types of cations in the perovskite composition.[42,46,47] However, the theoretical predictions for different perovskite compositions do not always lead to a stable and photoactive perovskite structure. Therefore, besides theoretical predictions, experimental proofs of concept are still useful to find optimized perovskite compositions. In addition to the mixed A-site cations, mixed metal cations and halides can also be considered for compositional combinatorial engineering of metal halide perovskite thin films, which are beyond the scope of this review.

Meanwhile, the field of colloidal perovskite NCs has received increasing attention owing to their high photoluminescence quantum yield (PLQY), facile synthesis, and enhanced stability over bulk thin films.[6,48–55] Over the last 7 years, research on perovskite NCs has explored their synthesis, surface chemistry, optical and electronic properties along with their applications.[6,14,50,56–58] The concept of A-site cation compositional engineering has also been extended to colloidal LHP NCs to fine-tune their optical properties as well as to improve their phase stability.[47,59–61] The mixed A-cation LHP NCs are of great interest for the fabrication of durable LEDs and solar cells.[14,47,61,62] Unlike bulk thin films, mixed A-site

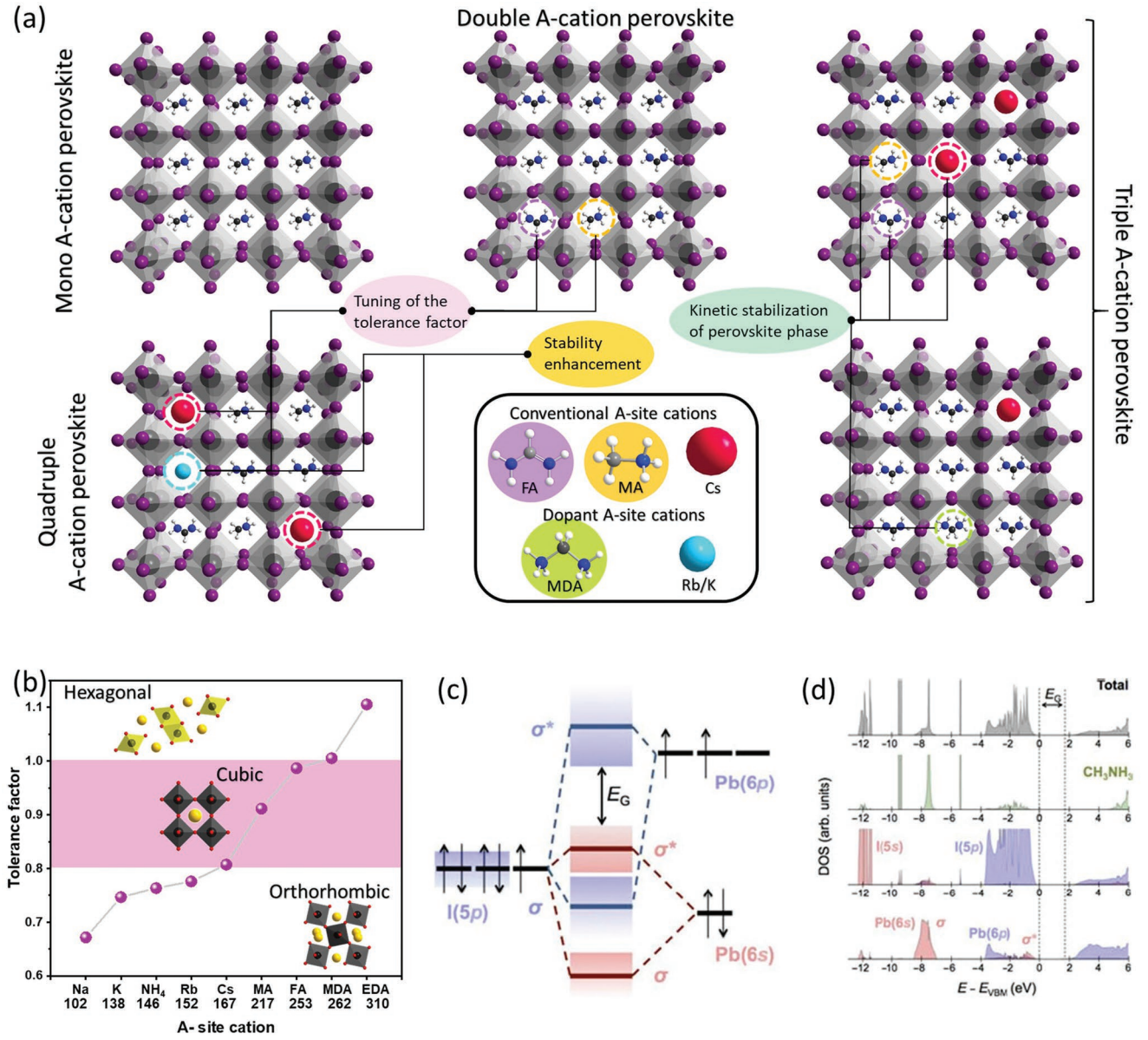

Figure 1. a) Schematic illustration of ABX_3 perovskite structure, as well as the full illustration of all possible multication combinations including single, double, triple, and quadruple components. b) Dependency of GTF of $APbI_3$ perovskites depending on A-cation radius. Colored part means region for stable cubic structure ($0.8 < t < 1$). The ionic radius values are obtained from ref. [39]. Figure is inspired by Refs. [64,65]. Note: There is a slight variation in the tolerance factors reported in different works due to differences in the ionic radii used for its calculation. c) Schematic illustration of the formation of bonding/antibonding orbitals in lead iodide perovskite through the hybridization of lead and iodide atomic orbitals. d) The calculated density of states (DOS) of $MAPbI_3$ differentiated into cation and anion s and p orbitals of iodide and lead. The A-cation does not introduce any new state at the band edge. Panels (c,d) are reproduced with permission.[40] Copyright 2015, The Materials Research Society.

cation LHP NCs can be prepared relatively easily through post-synthetic A-site exchange or cross-exchange similar to halide exchange.[47,59,63] In this review article, we first discuss the development of various types of mixed A-site cation and mixed cation perovskite thin-film systems developed over the years for improving the long-term stability of solar cells. The role of the A-site cation on the structure, optoelectronic properties, and halide migration in halide perovskites is discussed. We then provide an overview of the synthesis of mixed A-site cation colloidal LHP NCs and their application in solar cells and LEDs. Finally, we conclude with an outlook on future research directions of mixed A-site cation perovskite NCs that address the outstanding questions in the field.

2. A-Site Mixed Cation Perovskite Bulk Thin-Film Solar Cells

After the first emergence of PSCs,[3] huge research efforts were focused on engineering and fundamental understanding

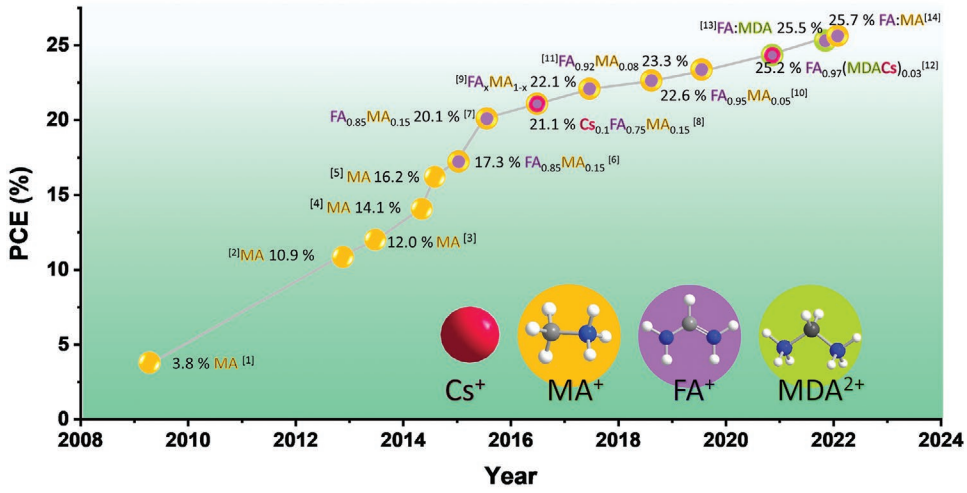

Figure 2. Some of the record PCE values reported for PSCs made of different A-cation compositions reported over the years (some of the data points obtained from NERL).[25] The data point number is given in brackets at each composition. The PCEs and the compositions are obtained from the references ((data point)[Ref.]:(1),[3] (2),[31] (3),[66] (4),[67] (5),[68] (6),[45] (7),[69] (8),[30] (9),[70] (10),[71] (11),[72] (12),[73] (13),[15] (14)[74]).

of this type of solar cells. Composition engineering of halide perovskites has been continually progressing during the PSCs development history to improve the PCEs and increase the device stability. However, introducing a new ion to a general ABX_3 perovskite composition can trigger unwanted effects such as phase segregation, emergence of lattice strain, and formation of vacancies and anti-site defects. Therefore, selecting a further ion for this purpose needs to be carefully pondered (both theoretically and experimentally) to achieve the best optoelectronic properties for the mixed perovskite compositions. Consequently, we review here the efforts made on A-site cation engineering in the perovskite crystal structure and its effect on the optoelectronic properties of perovskites with the aim of achieving highly efficient and stable PSCs. Regarding the PCE development of PSCs over the years,[25] except for the initial record for the pure $MAPbI_3$ with the PCE of 14.1%, most the best PCEs have been achieved for mixed A- and/or X-site hybrid perovskites, that is, mixed perovskites (**Figure 2**).[3,15,25,30,31,66–74] In this review, we limit our discussion to mixed A-cation perovskite systems. These systems with different combination A-cations are being intensively investigated across the globe to enhance the device operational stability, reproducibility, and PCE of PSCs. In this section, we provide a comprehensive discussion on the efficiency and stability progresses of thin-film PSCs by using different mixed cation perovskite systems such as double, triple, and quadruple A-Site cations.

2.1. Thin Films

At the beginning of the development of PSCs, ABX_3 perovskite compositions with single A, B, and X species (e.g., $MAPbI_3$, $FAPbI_3$, $CsPbI_3$, etc.) were extensively explored due to their simplicity. However, these perovskites have not delivered the highest PCEs and stabilities in PSCs.[75] For example, $MAPbI_3$ is one of the most explored simple single A-site cation perovskite compositions, but with this composition it is challenging to reach PCEs beyond 21%.[76,77] On the other hand, due to the hygroscopic and volatile properties of the MA^+ cation, this composition readily undergoes irreversible degradation and phase transition under ambient conditions such as moisture, oxygen, heat, and light, which limit the long-term operational and thermal stability of $MAPbI_3$ based PSCs.[78,79]

In this regard, FA^+ or Cs^+ cations have been used as alternatives for MA^+ in $MAPbI_3$, that is, $FAPbI_3$ and $CsPbI_3$, improving the solar cells operating temperature range to over 80 °C.[80,81] Apart from thermal stability, $FAPbI_3$ and $CsPbI_3$ provide bandgaps of 1.48 and 1.73 eV, respectively, which makes them excellent candidates for single-junction and tandem solar cells applications, respectively.[82] However, phase instability is a major challenge for these compositions because their black perovskite phases undergo a transition to a non-photoactive yellow phase at room temperature.[83,84] The fact that tilting angles of the $[PbI_6]^{4-}$ octahedra in all-inorganic $CsPbI_3$ can easily vary explains the existence of various crystal polymorph, that is, the cubic phase (α-, Pm3m), the tetragonal phase (-, P4/mbm), the orthorhombic phase (γ-, Pbnm) and an orthorhombic non-perovskite phase (δ-, Pnma). The possible formation of so many polymorphs influences the photovoltaic properties and device stability.[85] Similarly, $FAPbI_3$ has four types of crystal polymorph phases: cubic (α-, P3m1/Pm3m), trigonal (b-, P3/P4mbm), tetragonal (γ-, P4mbm), and hexagonal non-perovskite phase (δ-, $P6_3mc$), all leading to different optoelectronic properties.[84] Mixing cations and halides has become a hot topic to simultaneously improve both the structural stability and PCE of PSCs. In this section, we discuss the state-of-the-art of all possibilities of mixed-cation perovskites based on multiple substitutions on the A-site of the perovskite and their effect on efficiency and long-term stability of perovskites in solar cells.

2.1.1. Double A-Site Perovskites

The partial substitution of the A-site cation in $MAPbI_3$, $FAPbI_3$, or $CsPbI_3$ thin films has been exploited to control the phase, humidity, and thermal stability, as well as tune the optical

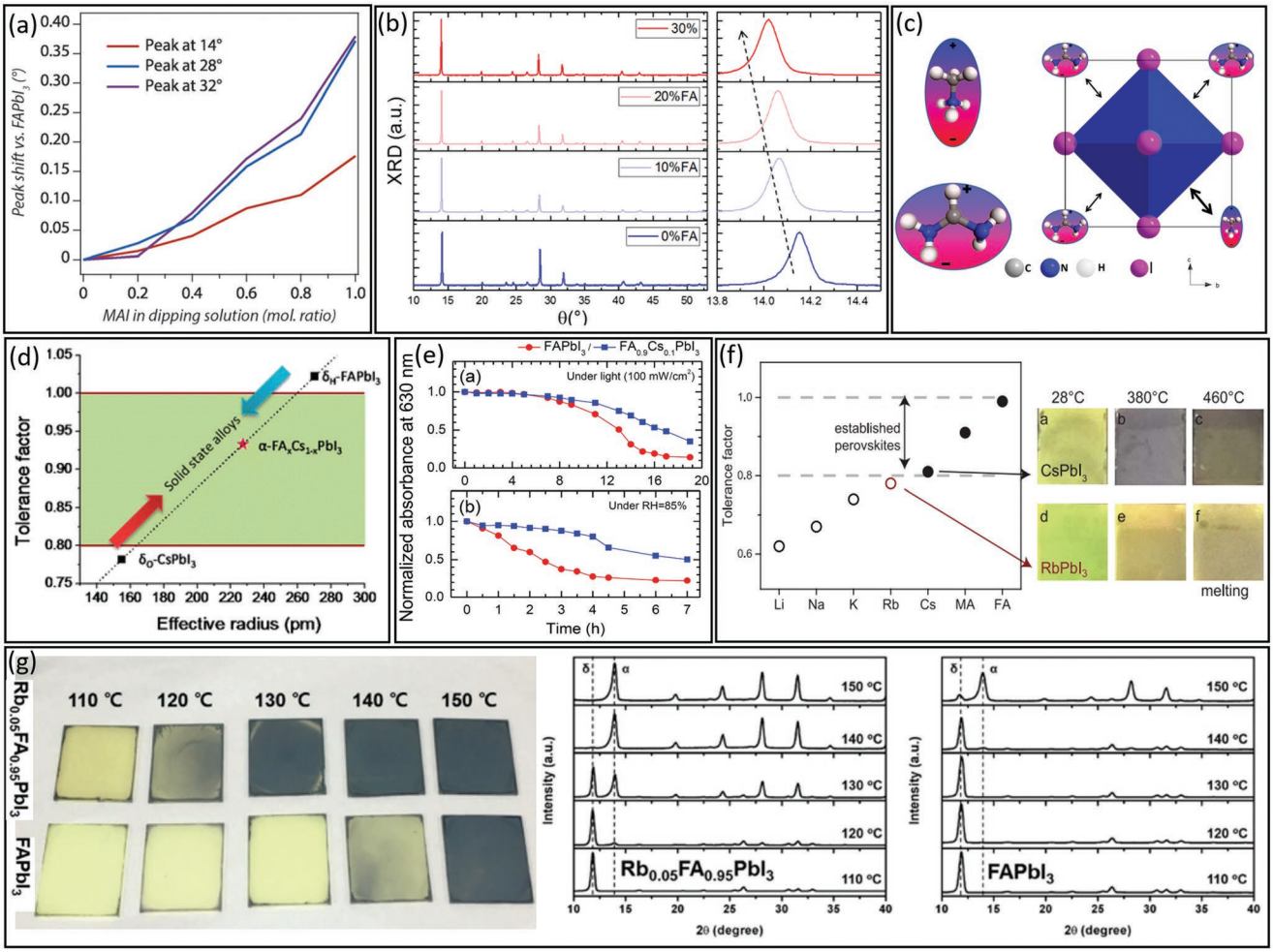

Figure 3. a) Summarized XRD peak shift of $(MA)_x(FA)_{1-x}PbI_3$ thin-film perovskites as compared to $FAPbI_3$ at 14°, 28.4°, and 31.88°. Reproduced with permission from Ref. [92]. Copyright 2014, Wiley-VCH. b) The XRD data and a zoomed-in view of the peak at 14° of $FA_xMA_{1-x}PbI_3$ films with different FA molar ratios. Reproduced with permission from Ref. [95]. Copyright 2017, American Chemical Society. c) Illustration of the influence of the MA and FA dipole moments on the inorganic cage of the perovskite structure. Reproduced with permission from Ref. [97]. Copyright 2015, American Chemical Society. d) The correlations between cation size and tolerance factor in the crystal structure of perovskite materials. Reproduced with permission from Ref. [37]. Copyright 2016, American Chemical Society. e) The normalized absorbance as a function of time from $FAPbI_3$ and $FA_{0.9}Cs_{0.1}PbI_3$ films under light (100 mW cm^{-2}) and severe humidity (RH = 85%). Reproduced with permission from Ref. [90]. Copyright 2015, Wiley-VCH. f) The influence of different cation sizes on the tolerance factor of $APbI_3$, as well as the phase transition of $CsPbI_3$ and $RbPbI_3$ at different temperatures. Reproduced with permission from Ref. [29]. Copyright 2016, The American Association for the Advancement of Science. g) Photograph and XRD patterns of the temperature dependence of phase transitions for $Rb_{0.05}FA_{0.95}PbI_3$ and $FAPbI_3$. Reproduced with permission from Ref. [101]. Copyright 2017, Wiley-VCH.

properties.[45,86–92] Although both pure MA- and FA-based perovskite compositions are sensitive to ambient conditions, the double A-site cation perovskites, that is, a mixture A site cation of MA^+ and FA^+, has shown a great potential to stabilize the crystal lattice.[18,93,94] In this regard, Grätzel et al. achieved a pure black phase of double-cation perovskites composition via the sequential deposition method by dipping the PbI_2 thin films in a solution of mixed FA^+ and MA^+ cations.[92] **Figure 3**a shows the XRD peak shift from pure α-$FAPbI_3$ to different MA^+ ratios in the double-cation system, specifically for the XRD peak at 14°, confirming the formation of a mixed phase of $(MA)_x(FA)_{1-x}PbI_3$) and the successful insertion of both cations in the same lattice frame. Additionally, they observed a red-shift in the absorption edge of pure α-$FAPbI_3$ by increasing the MA^+ cation ratio in the perovskite composition, confirming the intercalation of the MA^+ cation in the $FAPbI_3$ crystal lattice. As a result, the optimized double-cation perovskite composition of $MA_{0.6}FA_{0.4}PbI_3$ delivered a PCE of 14.9%, which is much higher than for pure $MAPbI_3$ and $FAPbI_3$ solar cells with the PCEs of 12.5% and 11.0%, respectively. On the other hand, Zhang et al.[95] demonstrated the improved crystallinity and compositional uniformity and thus enhanced PCE of $MAPbI_3$ perovskite by including 10% FA^+ cations (which have a larger size than MA^+). This is likely caused by the reduction of degradation pathways arising from MA and longer charge diffusion length, and a favorable band gap shift toward the ideal value. As shown in Figure 3b, the XRD peak position at the $2\theta = 14.1^\circ$ (see also the zoomed-in views), 20.0°, 24.4°, 28.4°, and 31.8° were shifted to lower angles, indicating the expansion of the crystal lattice and the stabilization of the perovskite in a "quasi cubic" phase

due to copresence of MA^+ and FA^+ in the mixed $FA_xMA_{1-x}PbI_3$ perovskite lattice. As a result, the $FA_{0.1}MA_{0.9}PbI_3$ composition showed better properties than pure $MAPbI_3$, such as higher crystallinity with a stable "quasi-cubic" phase at room temperature and a PCE beyond 20%.

Understanding the phase stabilization mechanism of different perovskite compositions is crucial for further composition engineering. For example, there are two possibilities to improve the α-phase stability of $FAPbI_3$. First, by increasing the number of hydrogen bonds between the ammonium moiety in the cation structure and the iodide ions in the $[PbI_6]^{4-}$ octahedra; second, by introducing different ammonium moieties with stronger hydrogen bonding capability. Regarding the first point, due to the limitation of fitting a maximum of four FA^+ cations in the perovskite cubic unit cells,[43] the number of hydrogen bonds will be identical for pure $FAPbI_3$ composition. However, based on the second strategy, using cations with different ammonium moieties can provide higher dipole moments, which leads to stronger hydrogen bonds with the iodide ions in the $[PbI_6]^{4-}$ units.[99] In this regard, Binek et al.[97] suggested that MA^+ with a higher dipole moment than FA^+ (2.3 D versus 0.21 D) forms stronger hydrogen bonds in the double cation system, leading to a stabilized α-$FAPbI_3$ structure. Different electron density configurations in the molecular structure of MA^+ compared to FA^+ are the reason for their different dipole moments. As shown in Figure 3c, the electron density in the FA^+ molecule is homogeneously distributed over the nitrogen-carbon-nitrogen bond, decreasing the dipole moment. In contrast, the electron density is non-homogeneously concentrated on the nitrogen atom in the MA^+ structure, which leads to a higher dipole moment in this molecule. As a result, the use of mixed FA/MA cation compositions has been established as an efficient strategy to achieve stable α-$FAPbI_3$ perovskite instead of high-temperature phase stabilization.

Unfortunately, the MA cation can leave the $MA_xFA_{1-x}PbI_3$ crystal structure due to its volatility, and this is at the base of low thermal and photostability of MA-based PSCs.[98] Alternatively, pure inorganic cesium-based perovskites have shown excellent thermal stability.[99] Moreover, the smaller ionic radius of Cs (1.81 Å) compared to MA (2.70 Å) and FA (2.79 Å) could suppress the formation of the yellow phase in mixed cation perovskite films compared to pure $CsPbI_3$ and $FAPbI_3$ by adjusting the tolerance factor in a way that is best suited for the cubic phase (Figure 3d).[37] Besides the phase stability, the $(Cs)_x(FA)_{1-x}PbI_3$ compositions have better thermal stability and photostability as well, which is due to shrinking of the cuboctahedral A-site by the small size of Cs^+, leading to stronger interactions of Cs with iodine atoms in the $[PbI_6]^{4-}$ octahedra and compressing unit cell dimensions.[90] In this regard, Park et al.[90] demonstrated that replacing 10% of FA^+ with Cs^+ in the pure $FAPbI_3$ composition, that is, $FA_{0.9}Cs_{0.1}PbI_3$, leads to a lower extent of photodegradation under constant illumination, as well as superior humidity stability under constant humidity of RH 85% (Figure 3e).

Rb with a smaller ionic radius of 1.52 Å than Cs (1.81 Å) can only stabilize the δ-phase for the pure $RbPbI_3$ composition. Saliba et al. demonstrated that δ-$CsPbI_3$ turns back to α-phase by heating up to 380 °C, while δ-$RbPbI_3$ remains unchanged at this temperature and even starts melting at 460 °C without turning to the α-phase (Figure 3f).[29] However, as a dopant, Rb could be considered another inorganic candidate for stabilizing the α-$FAPbI_3$ perovskite with improved crystallinity by obtaining double cation system $Rb_xFA_{1-x}PbI_3$.[29,100] In this regard, Park et al. traced the crystallization of the $FAPbI_3$ perovskite in the presence of a small amount of Rb cation.[101] As shown in Figure 3g, the film containing 5% Rb, that is, $Rb_{0.05}FA_{0.95}PbI_3$, turned to the black phase at 120 °C and completely darkened at 150 °C, while the phase conversion started at 140 °C for pure $FAPbI_3$, and completely darkened at 150 °C. The XRD patterns of the two compositions also confirmed the fact that introducing Rb into $FAPbI_3$ leads to phase conversion at lower temperatures compared to the pure $FAPbI_3$ (see Figure 3g). Therefore, in double cation perovskite systems, a small amount of Rb in the lattice could modify the tolerance factor in a way that helps the stabilization of photoactive phase, which is similar to other mixed A-cation systems (e.g., $Cs_xFA_{1-x}PbX_3$). Unfortunately, other alkali metals such as Li, Na, and K are too small to provide a pure or mixed double cation perovskite system.

Besides the small cations, the large guanidinium $[C(NH_2)_3^+$, GA] cation has also been used for stabilizing $MAPbI_3$ or $FAPbI_3$ perovskites.[102,103] Again, due to the big size of this cation, the pure Ga-based perovskite ($GAPbI_3$) exceeds the limit of the GTF ($t = 1.03$) and shows temperature-dependent phase instability.[104,105] However, the GA cation as a dopant in other perovskite compositions provides a high number of H-I bonds interacting with the $[PbI_6]^{4-}$ inorganic framework due to three ammonium groups in its molecular structure, leading to a more stable perovskite structure. For example, the PSCs made with $GA_{0.25}MA_{0.75}PbI_3$ composition showed excellent thermal stability and preserves 90% of their PCE for up to 300 h at 85 °C under inert conditions, whereas pure $MAPbI_3$ retains only 70% of the PCE under the same conditions.[109]

2.1.2. Triple A-Site Cation Perovskites

As discussed so far, the double cations system helps to stabilize the pure single cation perovskites, that is, $MAPbI_3$, $FAPbI_3$, and $CsPbI_3$. The MA cation plays an important role in FA/MA perovskites as crystallizer and black phase stabilizer. Despite high PCEs of FA/MA perovskites, obtaining a FA/MA perovskite without any trace of the yellow phase is always challenging, and this negatively affects the long-term device stability.[16,45,92,106,107] Therefore, developing new composition engineering approaches to achieve pure black phase in double cations system without affecting the other parameters is very important for further developments of PSCs. To address this challenge, Saliba et al. introduced triple cations FA/MA/Cs to improve further the properties of the double cation system.[30] As shown in **Figure 4**a, introducing small amounts of Cs (5–15%) to the FA/MA perovskite leads to the disappearance of the photoinactive hexagonal δ-phase and the cubic PbI_2 from the XRD pattern. This effect is due to a reduction of the effective cation radius in the new triple Cs/MA/FA system, pushing the tolerance factor towards the stable cubic α-phase perovskite. The triple cations perovskite films showed higher thermal stability and reproducibility regarding PEC compared

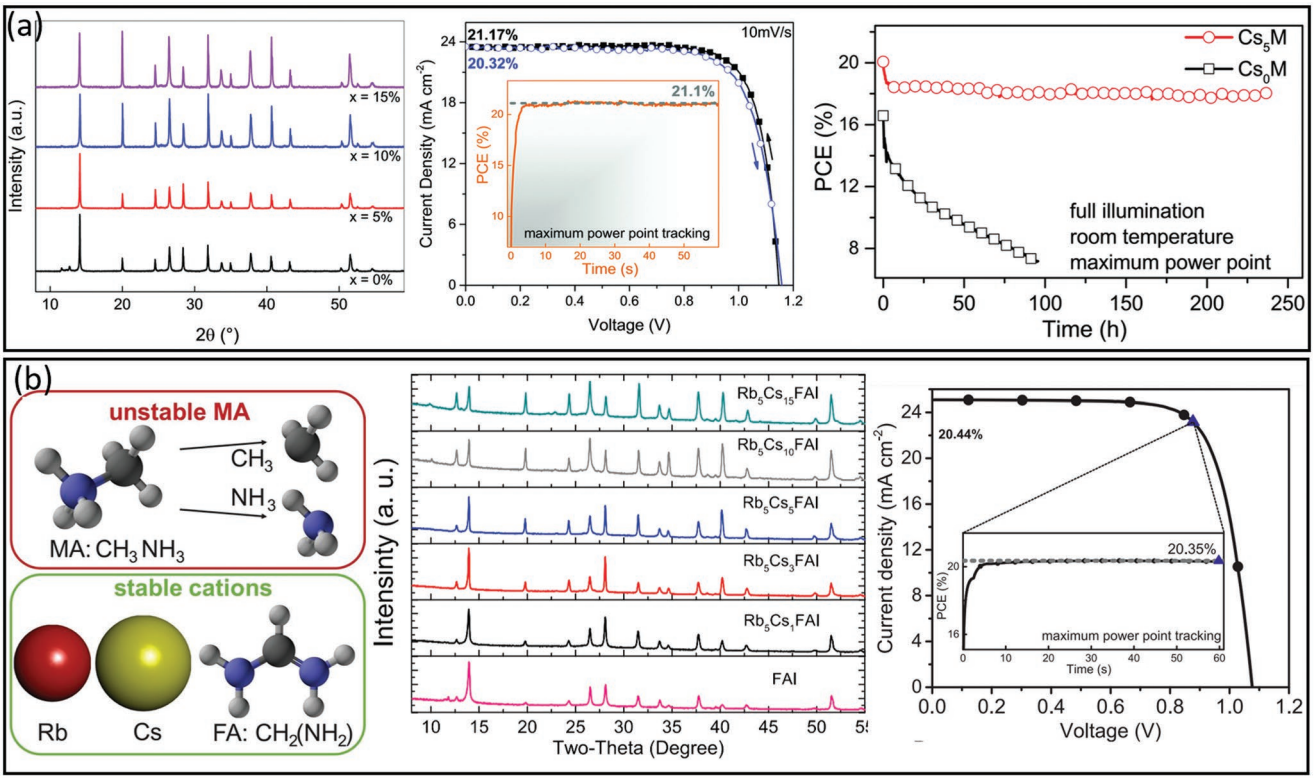

Figure 4. a) The XRD pattern of Cs_xM compounds, the champion J-V of Cs_5M, and long-term stability characterization of Cs_5M and Cs_0M devices under constant illumination and maximum power point tracking. Reproduced with permission from Ref. [30]. Copyright 2016, The Royal Society of Chemistry. For convenience, the composition "$Cs_x(MA_{0.17}FA_{0.83})_{(100-x)}Pb(I_{0.83}Br_{0.17})_3$" is abbreviated as Cs_xM (x is in percentage), where M means "mixed perovskite"; that is, Cs_0M stands for no Cs. b) Illustration of the MA molecule decomposition, and thermally stable Rb, Cs, and FA cations, as well as XRD pattern of different MA-free composition and the champion *J–V* of $Rb_5Cs_{10}FAPbI_3$ device. Reproduced with permission from Ref. [109]. Copyright 2018, The American Association for the Advancement of Science.

to the double cations counterpart, which is very crucial for the further development of cost-efficient manufacturing PSCs.[11] As a result, the triple cations-based PSCs delivered a high stabilized PCE of 21.1% and ≈18% after 250 h under operational conditions (Figure 4a). The Miyasaka group also confirmed the robustness of the Cs/MA/FA triple cation perovskite composition in terms of reproducibility, efficiency, and stability.[113] They demonstrated that high-quality triple perovskite films could even be prepared in ambient air (<RH 25%) without the need to operate in an inert atmosphere glove box, and that they were insensitive to different antisolvents by delivering almost identical film morphology when deposited from any of them. Moreover, the fabricated triple cations PSCs showed PCE of over 20% with outstanding long-term stability (up to 18 weeks) under ambient air with 20–35% relative humidity.[113]

The Cs/MA/FA triple cation perovskite became a very reproducible and favorable composition in the perovskite community. Yet, the presence of the highly volatile MA cation in this composition is considered a long-term risk for universalizing this composition. As shown in Figure 4b schematically, the MA itself starts to degrade to CH_3I and NH_3 at temperatures over 80 °C, which contrasts with ISOS protocol long-term stability test of PSCs at 85 °C (ISOS-D-2).[79] This has motivated scientists to identify new MA-free perovskite compositions to overcome the intrinsic instability of the perovskite films. In this regard, Saliba et al.[114] introduce a triple MA-free $Rb_xCs_yFA_{(100-x-y)}PbI_3$ composition that did not require annealing temperatures beyond 100 °C, providing a compatible path for flexible and perovskite/Si silicon tandem solar cells. As shown in the XRD data, increasing the amount of Cs (10–15%) in the Rb/FA double cation system leads to better crystallization of perovskite lattice and suggesting the formation of $RbCsPbI_3$ perovskites for some Rb/Cs ratios (this can be been seen as an additional phase at 10° region for 10 and 15% Cs) (Figure 4b).[114] These inorganic materials are expected to passivate the remaining pure $FAPbI_3$ perovskite layer. Moreover, the $Rb_5Cs_{10}FAPbI_3$ composition showed regular and compact film morphology, which is crucial to achieving high performance and reproducible solar cells. Therefore, Saliba et al.[114] emphasized that $Rb_5Cs_{10}FAPbI_3$ is a good trade-off between material with optimal bandgap (very close to $FAPbI_3$) and phase stability. As a result, the champion $Rb_5Cs_{10}FAPbI_3$-device showed a stabilized PCE of 20.3% with 1000 h stability under maximum power tracking (Figure 4b).

2.1.3. Quadruple A-Site Cation Perovskites

Further complexity in the A-cation composition has been introduced with an additional cation in triple-cations perovskites to

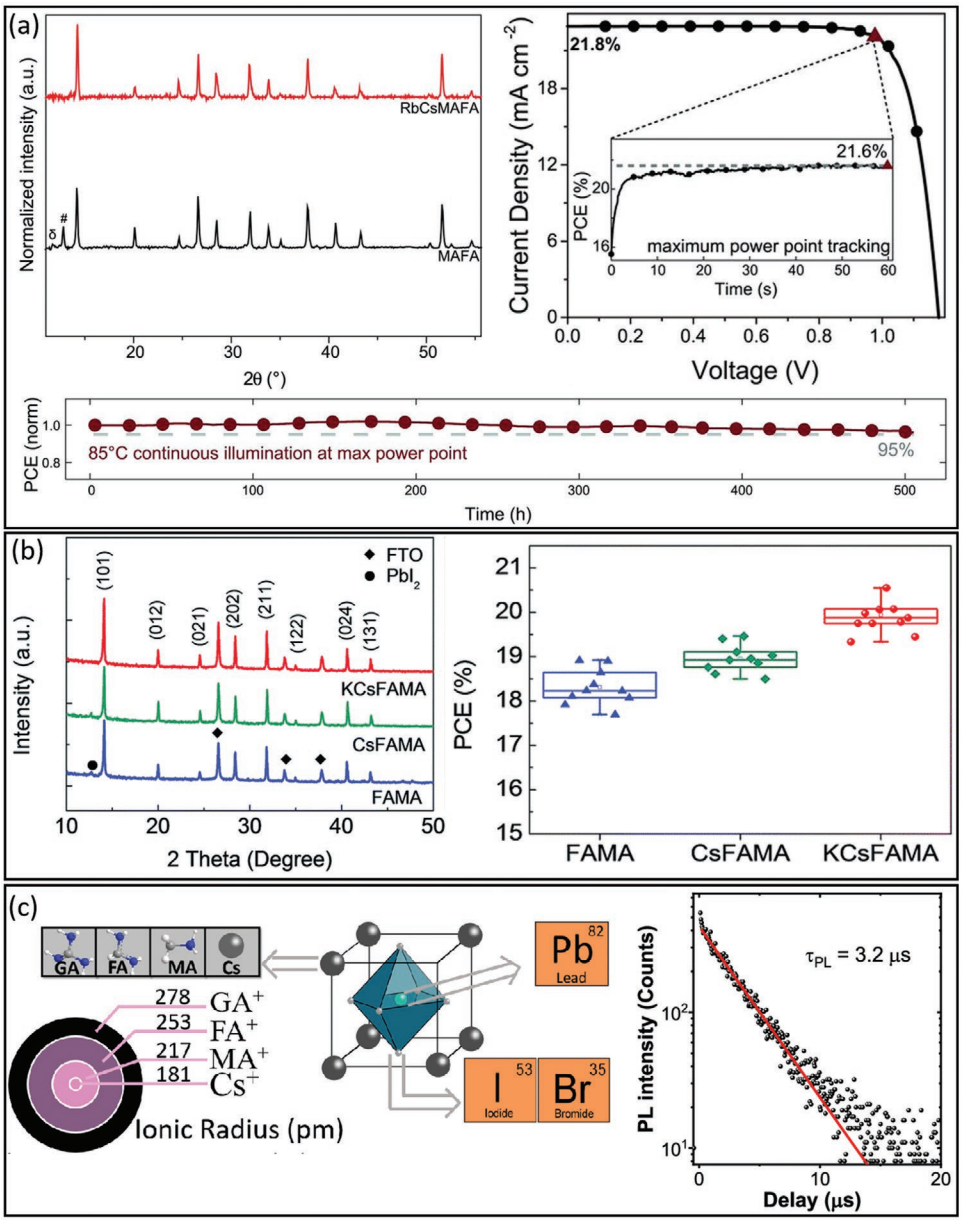

Figure 5. a) XRD data of the annealed MAFA and RbCsMAFA films, the champion *J–V* and thermal stability test of the optimized RbCsMAFA composition. Reproduced with permission from Ref. [29]. Copyright 2016, The American Association for the Advancement of Science. b) XRD patterns and PCEs of FAMA/CsFAMA/KCsFAMA perovskite films. Reproduced with permission from Ref. [112]. Copyright 2017, The Royal Society of Chemistry. c) Schematic representation of the ABX_3 perovskite unit cell with different A cations and TRPL data of the optimized GACsFAMA perovskite film. Reproduced with permission from Ref. [116]. Copyright 2020, American Chemical Society.

improve the stability and efficiency by increasing the entropy of the mixed composition. In this regard, Saliba et al.[29] were the first to introduce quadruple-cation perovskites by adding a small portion of Rb cations to Cs/MA/FA, that is, $Rb_x(CsMAFA)_{(100-x)}$ (x is in percentage), to enhance the already achieved stability and charge carrier transport for triple-cation perovskites. This increase in stability can be rationalized in terms of increased configurational entropy. The 5% Rb composition was identified as the optimal one (i.e., $Rb_{5\%}(CsMAFA)_{95\%}$) from XRD data, which evidenced the absence of peaks from PbI_2 and from the yellow phase. Also, the perovskite peaks were shifted to wider angles, indicating the reduction in lattice parameter caused by the Rb cations (**Figure 5**a). However, by increasing the fraction of Rb over 5%, the peaks related to the pure yellow-phase $RbPbI_3$ appeared, demonstrating the importance of precise composition engineering for achieving the photoactive phase. As a result, the fabricated PSCs with $Rb_{5\%}(CsMAFA)_{95\%}$ composition delivered a highly stabilized power output of 21.6% with V_{oc} deficit of only ≈0.39 V, that is, the difference between V_{oc} and bandgap, demonstrating the suppressed nonradiative recombination.[6,110] Moreover, besides this outstanding high efficiency, this robust Rb-based perovskite composition showed

high device stability under a harsh condition of 85 °C under continuous illumination at maximum power point (MPP) tracking for 500 h with 95% retention of its initial performance.

Potassium (K) is another cation that has been used as a dopant to improve the perovskite composition.[111,112] Similar to $RbPbI_3$, achieving the black phase of pure $KPbI_3$ perovskite is impossible due to the small K^+ ionic radius and the super low GTF (lower than 0.8) of the hypothetical $KPbI_3$ perovskite phase. However, Bu et al.[112] demonstrated that the potassium-containing quadruple-cation perovskite KCsFAMA shows improved optoelectronic properties compared to the triple-cation CsFAMA and double-cation FAMA perovskites. The XRD data demonstrated that incorporating the K cation improves the crystallinity and suppresses the formation of the unfavorable δ-phase (Figure 5b). As a result, the PSCs fabricated with quadruple KCsFAMA perovskite presented an average PCEs of over 20%, which is much higher than that of double and triple-PSCs (Figure 5b). Later, Abdi-Jalebi et al.[111] also demonstrated that potassium-containing triple-cation perovskite, that is, quadruple KCsFAMA, has enhanced radiative efficiency, even higher than the rubidium-based counterparts.

Besides the alkali metal cations, introducing the GA cation in triple-cation perovskite, that is, quadruple-cation GACsFAMA (Figure 5c), improves the optoelectronic properties by minimizing the nonradiative charge carrier recombination.[106,113–115] In this regard, Jung et al.[116] recorded a long carrier lifetime of 3.2 µs for quadruple-cation GACsFAMA perovskite composition and achieved photovoltaic efficiencies above 20% with high operational stability. They demonstrated that, in this composition, GA cations passivate the recombination centers at the grain boundaries and increase the lifetime of charge carriers drastically (up to the microsecond time scale). **Table 1** covers bandgaps, carrier lifetimes, all photovoltaic parameters, and device stabilities for the best efficiency records of each A-mixed cation composition.

3. The Role of the A-Site Cation on Structure, Optoelectronic Properties, and Halide Migration in Bulk Thin-Films

From the earlier sections, it can be seen that the A-site of halide perovskites, far from being an inactive part of the structure, has a strong influence on the optoelectronic properties, crystal structure, and photo-, environmental- and thermal-stability. In this section, we delve deeper into how the species present at the A-site influence these properties by analyzing the recent fundamental studies into these materials (both thin films and single crystals).

3.1. Controlling Octahedral Tilting and Alkylammonium Re-Orientational Dynamics

As discussed in Section 2, $FAPbI_3$ is desirable over $MAPbI_3$ for PV applications, owing to its higher thermal stability and lower optical bandgap (of 1.48 eV[19,80]) that is closer to the optimum value for single-junction solar cells than $MAPbI_3$ (1.55 eV[122]). However, the GTF exceeds 1 for $FAPbI_3$ owing to the large size of the FA^+ cations, and the hexagonal δ-phase readily forms at room temperature (space group: $P6_3mc$[84] or $P6_3/mmc$[123]). The photoactive α-phase of $FAPbI_3$ (space group: $Pm\bar{3}m$) can be formed when processed at high temperatures (>150 °C),[124] because the cubic arrangement of corner-sharing $[PbI_6]^{4-}$ octahedra is then entropically-stabilized by the isotropic random orientation of the FA^+ cations.[123] Developing strategies to suppress the transition to the hexagonal phase upon cooling to room temperature requires an understanding of the re-orientational dynamics of FA^+, how they influence octahedral tilting in the halide perovskite, and how the re-orientational modes can be controlled through alloying in the A-site.

The ball and stick molecular model of the FA^+ cation is shown in **Figure 6**a. Based on the geometry of this molecular cation, it is believed that the main re-orientational modes are: 1) 180° rotations about the axis connecting the two nitrogen atoms, and 2) 120° rotation perpendicular to the plane of the FA^+ molecule.[125] The modes accessible at different temperatures influence the degree of octahedral tilting and the structure of the lattice. On cooling down $FAPbI_3$, the phase changes from a cubic α-phase ($Pm\bar{3}m$) to a tetragonal β-phase (P4/mbm) at 285 K, followed by a further transition to a tetragonal γ-phase (P4/mbm) at 140 K[135] that has cubic pseudosymmetry. These structural transitions come about due to the changes in the tilting of the $[PbI_6]^{4-}$ octahedra, which occur along with reductions in the dynamic degrees of freedom of the FA^+ cation.[126,127] The tilting of the octahedra can be described using the Glazer notation (i.e., $a^xb^yc^z$), in which the letters *a*, *b*, and *c* refer to the three principal axes ([100], [010], and [001]), while the superscript can be 0 (no tilting), + (in-phase tilting), or − (anti-phase tilting).[128] For the high-symmetry α-phase, the Glazer tilt is $a^0a^0a^0$, reflecting the absence of octahedral tilting and high degrees of re-orientational freedom of the FA^+ cation. Upon cooling to the β-phase, the Glazer tilt is described as $a^0a^0c^+$, meaning that there is in-phase tilting along the *c*-axis. In the γ-phase, the Glazer tilt remains the same, although upon changing from β- to γ-phase, there is a discontinuous change in lattice parameter and Pb-I-Pb bond angle, along with a discontinuous blue-shift in the PL peak.[135] Upon cooling to room temperature, $FAPbI_3$ can also undergo a phase transition to the hexagonal δ-phase, owing to reductions in the rotational degrees of freedom of the FA^+ cations. But this phase transition to the δ-phase involves the breaking of Pb-I bonds, as well as the complex sliding and twisting of the constituent atoms. There is therefore an energy barrier between the δ- and α-phases, and the transition between these two phases depends on the heating and cooling rates.[123] That is, $FAPbI_3$ can be kinetically trapped in the α-phase at room temperature if it is rapidly quenched.[123]

It is suspected that further phase transitions occur in $FAPbI_3$ that are not crystallographically detectable, owing to changes in the re-orientational dynamics of FA^+. This has been found in $FAPbBr_3$, which undergoes two crystallographically-observable phase transitions (between cubic, tetragonal and orthorhombic),[127] but has an extra three phase transitions that are not observable from diffraction experiments, which are believed to arise from the formation of nanoscale domains due to the strain arising from geometric frustrations of the FA^+ quadrupoles. These extra phase transitions influence the

Table 1. Bandgaps, charge-carrier lifetimes, photovoltaic parameters, and photovoltaic device stabilities in terms of operational time (MPP: Maximum power point; SPO: Stabilized power output; RH: Relative humidity; Ar: Argon; N_2: Nitrogen) for some of the most efficient mixed A-site cation perovskite systems reported over the years.

Cation	Composition	Architecture	Bandgap [eV]	Carrier lifetime [ns]	V_{oc} [V]	J_{sc} [mA cm^{-2}]	FF [%]	PCE [%]	Stability	Ref.
MA	$MAPbI_3$	FTO/b-TiO_2/m-TiO_2/perovskite/Spiro-OMeTAD/Au	1.61	164	1.14	23.7	81.0	21.9	120 s SPO (N2)	[117]
FA/MA	$(FAPbI_3)_{1-x}(MACl)_x$	FTO/b-TiO_2/SnO_2 QDs/perovskite/OAI/spiro-OMeTAD/Au	1.53	221	1.17	26.0	83.8	25.7	350 h MPP(N2)	[74]
FA/MDA	$FAPbI_3$:0.38$MDACl_2$	FTO/SnO_2/$FAPbI_3$/Spiro-OMeTAD/Au	1.51	1426.7	1.18	25.7	83.2	25.5	500 h MPP(N2)	[15]
FA/Rb	$Rb_{0.05}FA_{0.95}PbI_3$	FTO/b-TiO_2/m-TiO_2/perovskite/Spiro-OMeTAD/Au	1.53	72.1	1.07	23.9	67	17.1	1000 h (RH 55%)	[118]
FA/Cs	$FA_{0.9}Cs_{0.1}PbI_3$	FTO/b-TiO_2/perovskite/Spiro-OMeTAD/Ag	1.55	N/A	1.07	23.4	76	19.0	200 h (RH 50%/T 65 °C)	[119]
MA/GA	$MA_{0.86}GA_{0.14}PbI_3$	FTO/b-TiO_2/m-TiO_2/perovskite/Spiro-OMeTAD/Au	1.77	N/A	1.08	23.2	80.3	20.1	1100 h (MPP/60 °C/Ar)	[103]
FA/MA/Cs	$Cs_5(MA_{0.17}FA_{0.83})_{95}Pb(I_{0.83}Br_{0.17})_3$	FTO/b-TiO_2/m-TiO_2/perovskite/Spiro-OMeTAD/Au	1.65	N/A	1.15	23.5	78.5	21.2	250 h (MPP/N2)	[30]
FA/MA/Rb	$Rb_{10}(MA_{0.17}FA_{0.83})_{90}Pb(I_{0.83}Br_{0.17})$	FTO/b-TiO_2/m-TiO_2/perovskite/PTAA/Au	1.61	98.04	1.25	23.2	71.9	18.8	100 h (MPP/N2)	[100]
FA/MDA/Cs	$(FAPbI_3)_{0.97}(MDACs)_{0.03}$	FTO/b-TiO_2/m-TiO_2/perovskite/Spiro-OMeTAD/Au	1.52	1609	1.17	26.2	82.1	25.2	400 h (MPP/ambient)	[73]
FA/Cs/Rb	$Rb_5Cs_{10}FAPbI_3$	FTO/SnO_2/PCBM:PMMA/perovskite/PMMA/HTM/Au	1.53	N/A	1.08	25.0	75	20.5	1000 h (MPP/N2)	[120]
FA/MA/Cs/Rb	$Rb_5Cs_{10}FAPbI_3$	FTO/b-TiO_2/m-TiO_2/perovskite/Spiro-OMeTAD/Au	1.63	N/A	1.18	22.8	81	21.8	500 h (MPP/N2/85 °C)	[121]
FA/MA/Cs/K	$K_x(Cs,MA,FA)Pb(I_{0.85}Br_{0.15})_3$	FTO/b-TiO_2/m-TiO_2/perovskite/Spiro-OMeTAD/Au	1.56	1500	1.17	23.2	79	21.5	400 h (MPP/N2)	[111]
FA/MA/Cs/K	$K_xCs_{0.05}(FA_{0.85}MA_{0.15})_{0.95}Pb(I_{0.85}Br_{0.15})_3$	FTO/SnO_2/perovskite/Spiro-OMeTAD/Au	1.59	239	1.13	22.9	79	20.5	1000 h (10%RH)	[112]
FA/MA/Cs/GA	$GA_{0.015}Cs_{0.046}MA_{0.152}FA_{0.787}Pb(I_{0.815}Br_{0.185})_3$	FTO/b-TiO_2/m-TiO_2/perovskite/Spiro-OMeTAD/Au	1.62	1500	1.18	23.6	75	20.9	3000 s (MPP/N2)	[116]

spectral-dependence of the photoconductivity, and as FA^+ motion is hindered at lower temperatures, the exciton-derived photocurrent is reduced.[140] These results emphasize the important role the motion of the organic cation plays on the optoelectronic properties of FA-based LHPs.

The phase transitions due to changes in the motion of the alkylammonium cation occurring in $FAPbI_3$ can also be found in $MAPbI_3$ (motion shown in Figure 6a). In the high-temperature cubic phase (also $Pm\bar{3}m$, with Glazer tilt of $a^0a^0a^0$), the MA^+ cation jumps between 8 equivalent positions, and this reduces to 4 positions upon cooling to the tetragonal phase (I4/mcm, Glazer tilt: $a^0a^0c^-$) at 330 K (Figure 6c).[125,130,132] At 160 K,[132] there is a phase transition to orthorhombic (Pbnm, Glazer tilt: $a^0b^-b^-$, Figure 6d), in which the MA^+ cation is frozen into a single antiferroelectric configuration, but still has the capability of hopping around its C_3 axis (Figure 6a).[130]

The re-orientation dynamics of both FA- and MA-lead halides and degree of octahedral tilting are influenced by mixing Cs^+ into the A-site, which has consequences on the phase-behavior of these alloys. For example, in $FAPbBr_3$, Neilson et al. found that adding as little as 5% Cs suppresses the four low-temperature phase transitions, preserving the P4/mbm phase down to at least 100 K.[136] The dynamic degrees of freedom of FA^+ are maintained with Cs^+ addition because the tilting preferences induced by both FA^+ and Cs^+ cations to the inorganic octahedra in lead-bromide perovskites are the

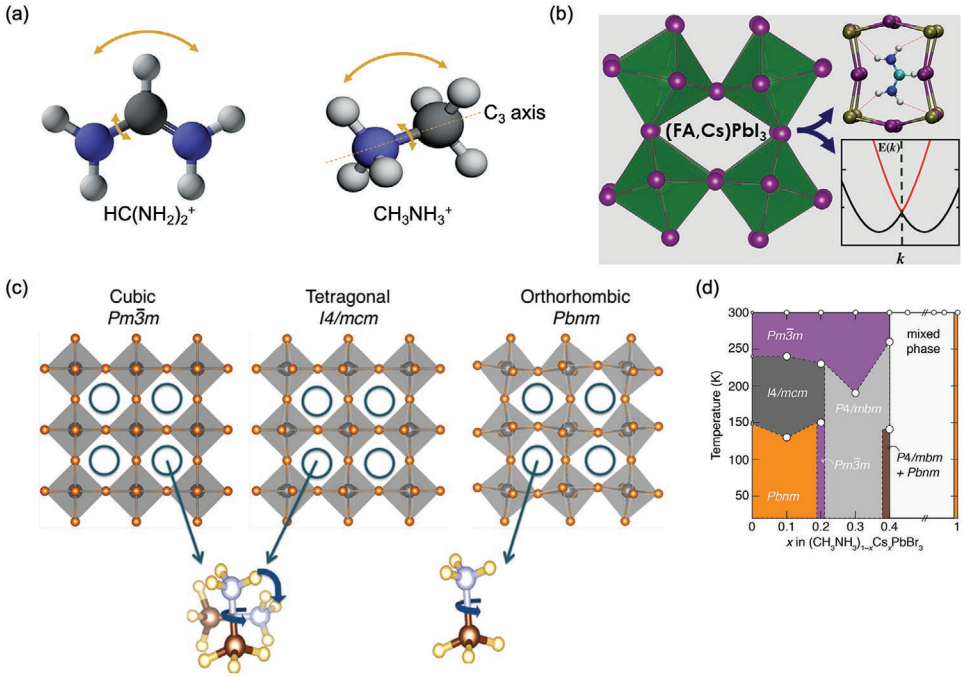

Figure 6. Influence of the re-orientational dynamics of $CH(NH_2)_2^+$ (FA^+) and $CH_3NH_3^+$ (MA^+) and on the properties of LHPs. a) Rotational modes and axes of rotation of FA^+ and MA^+.[125] b) Illustration of octahedral tilting in $FAPbI_3$ alloyed with Cs, the hydrogen bonding between the FA^+ and I^- anions in the inorganic octahedra, and the Rashba splitting resulting from the structural distortions with Cs alloying. Reproduced with permission.[129] Copyright 2018, American Chemical Society. c) Structure of $MAPbBr_3$ depending on the orientational modes accessible to MA^+ at different temperatures and d) phase diagram of the perovskites as a function of the degree of Cs alloying to the A-site. Parts (c) and (d) reproduced with permission.[130] Copyright 2017, American Chemical Society.

same. But it is believed that the changes to the phase behavior of this material stem from changes to the strain field introduced through the addition of Cs^+.[125,127] That is, FA^+ has a strong quadrupolar moment (where $|Q_{11}| = 3.6$ D) owing to the presence of the two electron-rich amine groups, and this leads to compressive and expansive strain fields being present due to the electrostatic interactions between the alkylammonium cation and the inorganic octahedral cages. These strain fields, which change depending on the orientation of the asymmetric FA^+ cations, play a role in the phase transitions in $FAPbBr_3$. By introducing compressive microstrains, the addition of Cs^+ leads to short-range ordering of the FA^+ quadrupole moments, thus overcoming the geometric frustration between the FA^+ cations, enabling the suppression of the lower-temperature phase transitions in $FAPbBr_3$. These results contrast with the behavior of MA^+, which has a strong electrostatic dipole (p = 2.3 D) but weak quadrupole moment ($|Q_{11}| = 3.6$ D).[127] Upon alloying $MAPbBr_3$ with Cs, the re-orientational dynamics of MA^+ are reduced due to the different octahedral tilting patterns induced by MA^+ versus Cs^+, such that mixed Cs-MA lead-bromide perovskites have been described as an orientational glass, which contrasts to the dynamically disordered plastic crystals of the pure MA-based perovskites.[125,127,130] The greater difficulty for MA^+ cations to reorient themselves results in sluggish phase transitions. Furthermore, the microstrain introduced through Cs addition leads to re-entrant phase transitions in the methylammonium-based perovskites, in which a cubic $Pm\bar{3}m$ phase forms instead of the orthorhombic Pbnm phase for sufficiently ≈20% Cs (Figure 6d).[130]

The findings described above by Neilson et al. for $FAPbBr_3$ contrast with the findings by Islam et al. for $FAPbI_3$. The latter reported, based on their computational analysis, that the addition of Cs to $FAPbI_3$ does indeed suppress the re-orientational dynamics of FA^+ owing to the strain arising from the size mismatch between Cs^+ (167–174 pm) and FA^+ (253 pm).[125,129] The strong hydrogen bonding between the amine groups in FA^+ and I^- anions in the inorganic octahedra result in structural distortions that suppress both the rotations of FA^+ and the dynamic tilting of the octahedra (Figure 6b). These computational results are in agreement with recent experimental results by Stranks et al. who showed that $FAPbI_3$ maintaining the photoactive a-phase through Cs-alloying exhibits octahedral tilting by approximately 2°, as observed from scanning electron diffraction patterns in TEM measurements, as well as nano-XRD measurements in a synchrotron.[124] Islam et al. further found that the structural distortions in Cs-FA perovskites break the symmetry of the lattice to give a Rashba-type effect, leading to an indirect bandgap that could lead to slower radiative recombination (Figure 6b).[129] Increasing the Cs content also leads to an increase in the bandgap, due to a lowering in the electron affinity and increase in the ionization potential. The increase in ionization potential was found to be due to the in-phase $[PbI_6]^{4-}$ octahedra tilting distorting the Pb-I-Pb bonds from an angle of 180°, such that there is reduced antibonding overlap between the Pb 6s and I 5p orbitals. The decrease in electron affinity is due to a symmetry-lowering distortion of the inorganic framework that leads to increased covalency in the otherwise ionic conduction band minimum.[138]

Regardless, the octahedral tilting induced by alloying into the A-site of $FAPbI_3$ has been found to be important for frustrating the transitions from the α- to δ-phase at room temperature. Scanning electron diffraction analysis of $FAPbI_3$ alloyed with both Cs and MA (i.e., triple cation perovskites) found that the unit cell had a lower-symmetry tetragonal structure (space group: P4/mbm) instead of a cubic phase, and that this tetragonal phase had a larger energy barrier against forming the hexagonal d-phase than the cubic phase did (75 meV versus 26 meV per formula unit, respectively). By using infrared nanospectroscopy to map the chemical signatures of FA and MA simultaneously to measure the morphology of the thin films, it was found that d-phase nanodomains (≈50–150 nm in size) still existed in the films. This was believed to occur due to local heterogeneities in A-site composition, such that locally FA-rich regions could form the hexagonal phase, which illustrates the drawbacks of inducing octahedral tilting in the perovskites through alloying.[124] It was found that these drawbacks could be addressed by using ethylenediaminetetraacetic acid (EDTA) as an additive to the precursor solution for $FAPbI_3$. NMR, NQR, and scanning electron diffraction analysis suggest that the bi-functional EDTA influenced the formation of the perovskite in solution and bound the surface of the films, but did not incorporate into them. By hindering the rotation of the FA^+ cations, the resulting perovskites were stabilized in the photoactive phase (as opposed to the hexagonal phase) at room temperature through octahedral tilting, that is, the $FAPbI_3$ formed had a space group of P4/mbm. The EDTA-stabilized films were found to be more stable against degradation to the d-phase in air than α-$FAPbI_3$.[124] Min et al. also reported the stabilization of the photoactive phase of $FAPbI_3$ through doping with MDA dichloride ($MDACl_2$), and this led to PVs with certified 23.7% efficiencies. It is possible that the $MDACl_2$ played a similar role through inducing octahedral tilting, but the macroscopic X-ray diffraction (XRD) measurements made were not able to detect small tilts.[19]

3.2. Influence of A-Site Composition on Halide Migration

Beyond the effect of the A-site cation on the phase of the perovskite and charge-carrier recombination rate, the species present at the A-site also influence halide migration.[133] It has been found by many authors that for mixed iodide-bromide perovskites, having MA in the A-site leads to rapid phase segregation, whereas using a mixture of Cs and FA (with 10–30% Cs) leads to much slower phase segregation.[34,133–136] This can be seen from the PL measurements shown in **Figure 7**a,b. When $MAPb(Br_{0.5}I_{0.5})_3$ thin films were photoexcited with a 470 nm wavelength continuous wave (cw) laser with a power density of 190 mW cm^{-2} (slightly above 1-sun), a red-shift in the PL peak occurred over the course of 15 min (Figure 7a), whereas $FA_{0.83}Cs_{0.17}Pb(Br_{0.4}I_{0.6})_3$ films photoexcited under identical conditions took 6 h to phase segregate to a similar degree (Figure 7b).[133] By contrast, the XRD pattern of $MAPb(Br_{0.5}I_{0.5})_3$ measured simultaneously with its PL measurement showed no shift in peak positions but only a decrease in intensity (Figure 7c) and an increase in the tail of the XRD peaks (Figure 7c, inset). For $FA_{0.83}Cs_{0.17}Pb(Br_{0.4}I_{0.6})_3$, on the other hand, the XRD pattern exhibited a shift towards lower 2q angles, but with a smaller

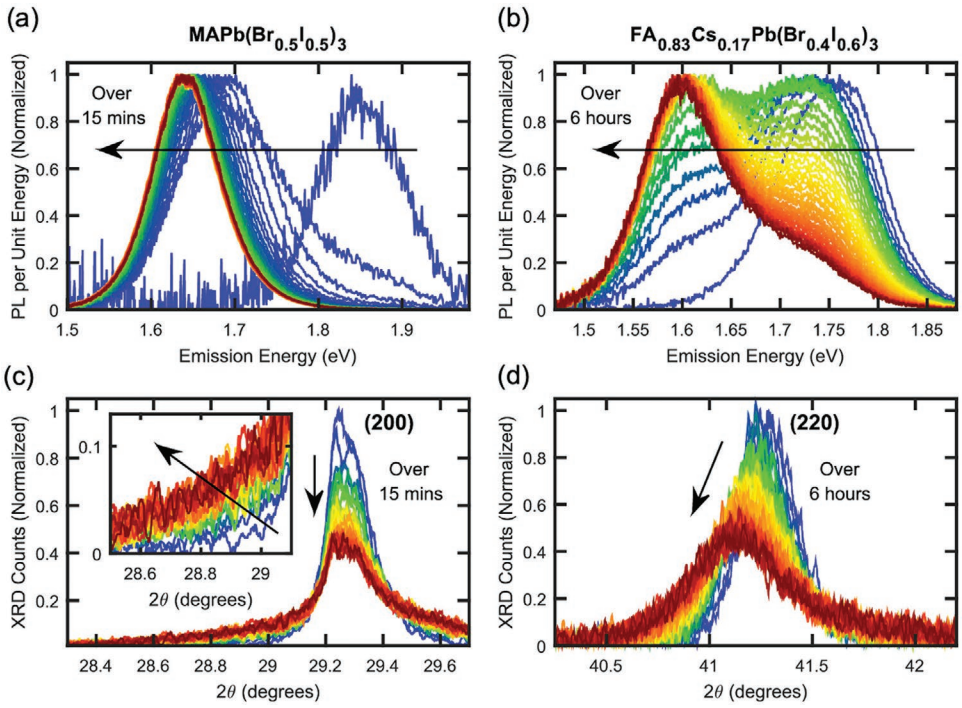

Figure 7. Halide segregation in MA versus FA-Cs mixed-halide perovskites. a,b) normalized PL spectra and c,d) selected XRD peaks of a,c) $MAPb(Br_{0.5}I_{0.5})_3$ and b,d) $FA_{0.83}Cs_{0.17}Pb(Br_{0.4}I_{0.6})_3$ perovskites. In parts (a) and (b), the perovskite films are coated with PMMA and excited with a wavelength of 470 nm, with an intensity of 190 mW cm^{-2}. The XRD peaks are measured using Cu K_a radiation. Reproduced with permission.[133] Copyright 2021, American Chemical Society.

change in the tails of these peaks (Figure 7d). The proposed model is that $MAPb(Br_{0.5}I_{0.5})_3$ undergoes halide segregation in minority regions (e.g., near grain boundaries where ionic motion can be faster), which propagates, causing the wider material to de-mix. This accounts for the rapid red-shift in PL as photo-excited carriers diffuse to reach the iodide-rich phases that form, but the absence of a shift in the main XRD peaks as the bulk material remains unchanged initially. By contrast, it is proposed that $FA_{0.83}Cs_{0.17}Pb(Br_{0.4}I_{0.6})_3$ lacks regions that are particularly susceptible to ion migration. Instead, for the material to de-mix, this needs to occur throughout the bulk in unison, which accounts for the red-shift in PL occurring over a longer timescale, and simultaneously to observable shifts in the XRD patterns. This slower bulk de-mixing is proposed to initiate following the segregation of the A-site cations, since the FA- or Cs-rich phases have been shown to be more susceptible to phase segregation, especially when the Cs content falls below ≈10% or above 30%.[133,135] It is suggested that the increased susceptibility of Cs-poor or Cs-rich FA-Cs perovskites, as well as MA-based perovskites, to phase segregation may arise partially from their lower crystallinity[135,136] or higher grain boundary density.[133]

From these studies, it appears that halide phase segregation could be suppressed by having larger grains and suppressing A-site cation segregation in mixed FA-Cs perovskites. A recent study by Pavlovetc et al. investigating triple-cation pure-iodide perovskite thin films showed that FA^+ and MA^+ diffusion could be suppressed through inclusions of orthorhombic d-phase $CsPbI_3$. These δ-phase inclusions were introduced by having higher concentrations of CsI in the triple-cation perovskite precursor solution. It is believed that this occurs because the δ-phase forms on the surface of α-phase triple-cation perovskite grains, forming a core-shell structure that inhibits MA/FA migration across grains.[137] Whilst the α/δ-phase mixture leads to improved solar cell operational stability, the PCE is lower due to inferior V_{OC}, J_{SC}, and FF.[137] Thus, alternative strategies need to be developed to suppress A-site cation segregation that does not compromise on performance.

3.3. A-Site Cation Migration

The A-site cation can also migrate in the presence of an electric field, and this can lead to demixing under operation, which can limit the operational stability of photoactive devices.[138] A-site cation migration usually has a higher activation energy barrier than anion migration, implying that these processes occur over a longer timescale,[139] which has been found experimentally to be on the order of $>10^3$ s (whereas halide vacancies migrate on the order of 10^{-1}–10^2 s).[140] But similar to anion migration, cation migration is believed to proceed via mobile cation vacancies, such as methylammonium vacancies.[140,141] Cation migration leads to device hysteresis and absorber degradation, and it is important to understand how this occurs and could be mitigated.

Several groups have performed controlled studies to investigate the role of A-site cation migration on the hysteresis in the performance of photovoltaics and photodetectors.[137,140–143] In photovoltaics, hysteresis is manifest in the PCE being dependent on the current–voltage (*I–V*) sweep direction, rate, sweep history, and any pre-conditioning treatments.[144] The level of hysteresis is often quantified by the hysteresis index ($HI = \frac{PCE_{reverse} - PCE_{forward}}{PCE_{reverse}}$), which can be as high as 0.4 for untreated triple-cation perovskites in standard *n-i-p* device structures.[143] Similarly, photodetectors demonstrated differences in the light and dark current depending on the scan direction and rate.[141] It has been observed that hysteresis is more severe at lower scan rates, which was attributed to charged defect ions migrating slower than charge-carriers, and therefore being favored to migrate at slower scans.[141] Poling experiments have been performed to experimentally observe the migration of ions by applying a bias across a pair of parallel electrodes on top of or beneath the film and characterizing the area between the electrodes.[137,142–143] Through infrared photothermal heterodyne imaging (IR-PHI) of the channel after poling, Pavlovetc et al. showed that $FA_{0.85}Cs_{0.15}PbI_3$ develops an inhomogeneous A-site cation distribution after biasing the parallel ITO electrodes for 60 min, in which the FA^+ cation species accumulate next to the negative electrode.[137] Similar behavior was found for $FA_{0.76}MA_{0.15}Cs_{0.09}PbI_3$, in which both FA^+ and MA^+ accumulated at the negative electrode and were depleted next to the positive electrode.[137] EDX and photothermal induced resonance microscopy of $MAPbI_3$ by Lin et al. also showed that MA^+ accumulated at the negative electrode, while I^- accumulated at the positive electrode following poling at 4 V μm^{-1} for 300 s.[142] The accumulation of cations (anions) at the interface with the electron (hole) transport layers of the perovskite devices results in electric field screening and changes in the charge-carrier extraction efficiency, hence the hysteresis observed in *I–V* sweeps of perovskite photovoltaic devices.[145] Similarly, in photodetectors, the accumulation of cations (anions) at the cathode (anode) in perovskite/Pt junctions leads to asymmetric Schottky barriers that give rise to hysteresis in the *I–V* curves.[141]

A number of strategies have been developed to mitigate A-site cation migration, including surface passivation,[146] the use of mixed phases,[137] and doping with alkali cations.[111,143] For example, Pavlovetc et al. showed that increasing the fraction of MA and Cs in triple-cation perovskites (forming $FA_{0.33}MA_{0.33}Cs_{0.33}PbI_3$) led to the formation of a mixture of α-phase perovskite (≈61%) and orthorhombic δ-phase (δ_o) $CsPbI_3$ (≈39%). IR-PHI measurements, along with time-of-flight secondary ion mass spectrometry (ToF-SIMS) measurements showed that laterally poling this mixed-phase material led to no A-site cation segregation, thus resulting in no shifts in the PL emission wavelength after biasing.[137] Cao et al. investigated doping Cs-, MA- or FA-based perovskites with Li^+, Na^+, K^+, or Rb^+, finding that at sufficiently low concentrations, these alkali cations occupy interstitial sites, leading to an increase in the activation energy barrier for halide ion migration. Whilst a larger alkali led to increased activation energy barriers to ion migration, there was also a smaller range of concentrations that could be doped into the interstitial sites.[152] Another factor that has been found to influence the migration of halide ions, as well as cations, is the presence of excess photogenerated charge-carriers. Lin et al. found that including an electron transport layer material (e.g., PCBM) onto the perovskite film to obtain excess photogenerated holes (by quenching electrons)

led to increased cation migration. It was speculated that this occurred because the excess holes neutralized the negatively-charged cation vacancies to reduce the Coulombic interactions between the ion and vacancy, enabling faster ion transport.[151]

A-site cation migration has also been found to limit the operational stability of photovoltaic devices. In situ XRD measurements on double- and triple-cation perovskite photovoltaic devices under operation have shown that the absorber phase-separates to the yellow hexagonal δ-phase (δ_h) $FAPbI_3$ and δ_o $CsPbI_3$, leading to a decrease in PCE. An important parameter that determines phase-stability is the Gibbs free energy of mixing (ΔG_{mix}), in which a negative ΔG_{mix} shows a mixed-cation alloy to be stable compared to the pure-A-site counterparts. Analyses by Schelhas et al. showed that mixed Cs-FA perovskites have less negative ΔG_{mix} values than MA-FA perovskites or triple-cation perovskites (with <10% Cs), which is consistent with the Cs-FA perovskites being less stable under operation.[147] These results are consistent with recent work by Li et al., which showed that whilst $FA_{0.9}Cs_{0.1}PbI_3$ is thermally stable, photovoltaic devices demonstrate poor operational stability (when under illumination and held at the maximum power point) owing to the demixing of the perovskite to form photoinactive Cs-rich clusters.[148] X-ray induced beam current measurements showed that these Cs-rich clusters resulted in reduced current collection, and hence reduced photovoltaic performance.[148] It was found that a higher density of these current-blocking Cs-rich clusters formed following illumination. Through DFT calculations, Li et al. found that when the population of photogenerated carriers was sufficiently large, the ΔG_{mix} becomes positive, leading to demixing.[157]

3.4. Influence of A-Site Composition on Charge-Carrier Dynamics

Apart from the influence on structure and ion migration, the A-site composition also plays an important role in carrier dynamics.[149–153] Chen et al. investigated the role of cations on hot carrier (HC) cooling in perovskite nanocrystals (NCs).[152] They claimed that the HC cooling time (τ_C) is influenced by the A-site cation composition in MHP NCs, where it was observed that τ_C decreased as the A-site changed from Cs to MA to FA in perovskite NCs, that is, $CsPbBr_3$ (390 fs) >$MAPbBr_3$ (270 ps) > $FAPbBr_3$ (210 fs).[152] A shorter τ_C in hybrid perovskites ($FAPbBr_3$ and $MAPbBr_3$) compared to that in the Cs-based MHP is attributed to stronger carrier–phonon coupling facilitated by the vibrational modes of the organic cations.[154,155] The role of molecular vibrations on HC relaxation was confirmed by the ability to slow down the cooling process at lower temperatures for $FAPbBr_3$. No effect, or a less marked effect, was observed for $CsPbBr_3$ NCs.[155] Wang et al. systematically studied the effect of mixed A-site cations (incorporating K^+, Rb^+, and Cs^+ cations into $(MAPbBr_3)_{0.17}(FAPbI_3)_{0.83}$ thin films) on HC cooling.[153] The synergetic effects from the Rb, Cs, and K cations resulted in a ≈900 K increase in the effective carrier temperature at a carrier density around 10^{18} cm^{-3} with an excitation 1.45 eV above the bandgap. In the doped thin films, particularly the $(Rb,Cs,K,MA,FA)Pb(Br,I)_3$ thin films, a carrier temperature greater than 600 K could be maintained over a time scale of >10 ps at a distance over hundreds of nanometers, which has the potential for achieving a PCE >45% in an HC solar cell.[153]

Besides the impact on charge-carriers above the band-edge, the A-site composition can also influence the charge-carriers at the band-edge. Nakanishi et al. reported the effect of mixed cations (Guanidium, Formamidinium, and Phenylethylamine) in tin iodide perovskites on their charge-carrier dynamics and performance in photovoltaics using time-resolved microwave conductivity (TRMC) measurements.[149] They found that, in $(GA_xFA_{1-x})_{0.9}PEA_{0.1}SnI_3$ films, the best solar cell was achieved with $x = 0.15$. At this composition, most of the GA cations were neither included in the grain nor they caused a significant change in the VBM and E_g but would be located on the grain surface, which would passivate the grain surface and improve μ_e. The further addition of GA ($x \geq 0.5$) led to its inclusion into the bulk of the grain and decreased both μ_e and μ_h.[149] Similarly, Saidaminov et al. claimed that the A-site composition can influence the carrier diffusivity across the grain boundaries.[156,157] They reported that methylammonium (MA)-based films show a high carrier diffusivity of $0.047\,cm^2\,s^{-1}$, while MA-free mixed Cs-FA perovskite films exhibit an order of magnitude lower diffusivity. Elemental composition studies show that Cs-FA grains display a graded composition. This curtails electron diffusion in these films, as seen in both vertical carrier transport and surface potential studies. Incorporation of MA leads to a uniform grain core-to-edge composition, giving rise to a diffusivity of $0.034\ cm^2\ s^{-1}$ in triple-cation perovskite films.[156] Apart from the influence on grain boundaries in thin films, which significantly influence the charge-carrier dynamics and transport, greater understanding is needed on the relationship between A-site composition and lattice strain and organic molecule reorientation at A-site, and how these factors could play a role in carrier dynamics.[150,158,159]

To summarize Section 3, it can be seen that the re-orientation dynamics, shape, dipole moment, and quadrupolar moment of the A-site cation has a significant influence on the structural and optoelectronic properties of LHPs. For example, these factors influence the tilting of the inorganic octahedra, and the phase transitions that can occur. There is disagreement in the literature on the specifics of how mixing Cs with an alkylammonium cation into the A-site influences the re-orientation dynamics of the alkylammonium cation and the band structure of the perovskite, but recent work has shown the importance of achieving a uniform mixture to prevent local non-radiative recombination sites or phase-segregation. This, however, may be unavoidable, and the use of pure FA or pure MA in the A-site, along with judiciously-chosen ligands to achieve octahedral-tilt-stabilized a-phase perovskite may be a more promising route to achieve high radiative efficiencies and avoid phase segregation in mixed-halide compositions.

4. Mixed A-Cation Halide Perovskite NCs

4.1. Synthesis

The successful demonstration of mixed A-cation halide perovskite thin films as photosensitizers in the fabrication of stable and reproducible solar cells has inspired the researchers to explore highly emissive and phase-stable colloidal mixed

A-cation LHP NCs.[14,47,59,61] These NCs have received increasing attention in recent years owing to their potential use as stable light emitters and photosensitizers in LEDs and solar cells, respectively.[14,47,59,61,160–162] In principle, the mixed inorganic and organic A-cation perovskite NCs possess the combined advantages of their individual counterparts. For instance, the mixed organic and inorganic A-cation systems merge the advantages of the superior stability of the inorganic part and the high solar cell efficiency of the organic counterpart. In addition, colloidal LHP NCs offer higher photoluminescence (PL) efficiency and superior stability as compared to their thin-film counterparts because of the capping ligands that passivate the NC surfaces. The higher phase stability (compared to mono A-cation LHP systems) along with high PLQYs makes the mixed A-cation LHP NCs promising materials for LEDs.[59,161,162] Furthermore, few recent reports demonstrated that these NCs are encouraging materials for the realization of stable and efficient PSCs.[14,47,61,160] However, unlike thin films, colloidal LHP NCs with precise tunability of the A-cation composition are relatively less explored.[14,75] The mixed A-cation perovskite NCs can be classified into three categories: 1) all-inorganic if the A-cation composition is made of Cs^+, Na^+, K^+, and Rb^+,[163–170] 2) all-organic if the A-cation composition is made of a mixture of MA^+ and FA^+,[171,172] 3) organic–inorganic hybrid if the A-cation composition is made of both organic and inorganic cations.[47,59–61,160,173,174] The most common mixed A-cation perovskite NCs consist of different combinations of Cs^+, MA^+, and FA^+.[47,59–61,160,173,174] It is important to note that the position of Na^+, K^+, and Rb^+ cations in the perovskite NC lattice is currently under debate. A few reports claimed that these cations occupy the A-sites, while most reports proposed that they occupy interstitial sites of the perovskite lattice. Therefore, the correct nomenclature for these Na^+, K^+, and Rb^+ doped/alloyed systems is "mixed-monovalent cation" perovskite NCs, and this applies to thin-film perovskites as well. **Table 2** summarizes different

Table 2. Literature overview of mixed A-cation (Cs^+, FA^+, MA^+) LHP NCs, and Na^+, K^+, and Rb^+-doped LHP NCs along with their composition, synthesis method employed, PL emission range, and PLQY. It should be noted that the position of the Na^+, K^+, and Rb^+ dopants in LHP NCs is under debate. Some reports claimed that they occupy interstitial sites while few reports claimed that they replace A-cations of the LHPs. Therefore, these systems belong to monovalent cation doped LHP NCs instead of mixed A-cation NCs.

Composition	Year	Synthesis method	Emission range [nm]	Tunability strategy	PLQY [%]	Ref.
$Na:CsPbBr_3$	2019	LARP	505–525	Precursor composition	44–85	[168]
$Na:CsPbBr_3$	2021	Hot injection	514–525	Precursor composition	50.4–94.2	[169]
$Cs_{1-m}K_mPbCl_3$	2018	Hot injection	408	Precursor composition	3.2–10.3	[183]
$K:CsPbBr_3$	2020	Hot injection	520–530	Precursor composition	48–84	[165]
$K:CsPb(Br_{1-m}Cl_m)_3$	2020	LARP	465–472	Precursor composition	9.5–38.4	[166]
$Cs_{1-m}Rb_mPbBr_3$	2018	Hot injection	474–532	Precursor composition	–	[179]
$Cs_{1-m}Rb_mPbBr_3$	2018	Hot injection	505–516	Precursor composition	93	[163]
$Cs_{1-m}Rb_mPbBr_{1.5}Cl_{1.5}$	2018	Hot injection	450	Precursor composition	86	[163]
$Cs_{1-m}Rb_mPbBr_3$	2018	Hot injection	500–513	Precursor composition	35–60	[170]
$Cs_{1-m}Rb_mPbCl_3$	2018	Hot injection	395–407	Precursor composition	2–10	[170]
$Cs_{1-m}Rb_mPbBr_3$	2019	Hot injection	465–510	Precursor composition	60–93	[184]
$Cs_{1-m}Rb_mPbBr_3$	2020	Hot injection	468–516	Precursor composition	–	[167]
$Rb:CsPb(Br_{1-m}Cl_m)_3$	2021	Sol-gel	457–510	A-cation and halide Exchange	20–60	[164]
$Cs_{1-m}MA_mPbBr_3$	2017	LARP	533–539	Precursor composition	–	[161]
$Cs_{1-m}MA_mPbI_3$	2017	Precipitation	720–826	Precursor composition	–	[174]
$Cs_{1-m}MA_mPbBr_3$	2021	LARP	506–509	Precursor composition	35.8–85.3	[185]
$Cs_{1-m}FA_mPbBr_3$	2017	LARP	519–538	Precursor composition	56–85	[181]
$Cs_{1-m}FA_mPbBr_3$	2017	LARP	519–531	Precursor composition	34–60	[173]
$Cs_{1-m}FA_mPbI_3$	2018	Hot injection A-cation exchange	690–780	Precursor composition/A-cation addition	>70%	[59]
$Cs_{1-m}FA_mPbI_3$	2018	A-cation exchange	650–800	NCs ratio	–	[47]
$Cs_{0.5}FA_{0.5}PbI_3$	2020	A-cation exchange	750	–	23–68	[61]
$Cs_{1-m}FA_mPb(Br_{1-m}I_m)_3$	2019	Simultaneously A- and X-site exchange	515–775	NCs ratio	–	[160]
$MA_{1-m}FA_mPbBr_3$	2017	LARP	460–565	Precursor composition	60–75	[172]
$MA_{1-m}FA_mPbBr_3$	2018	LARP	528–531	Precursor composition	87–89	[171]
$(Rb_{0.33}Cs_{0.67})_{0.42}FA_{0.58}PbBr_3$	2019	Hot injection/multi cation hot injection method	500	–	64.5	[186]
$(Rb_{0.33}Cs_{0.67})_{0.42}FA_{0.58}PbCl_{1.25}Br_{1.75}$	2019	Hot injection/multi cation hot injection method	476	–	49.8	[186]

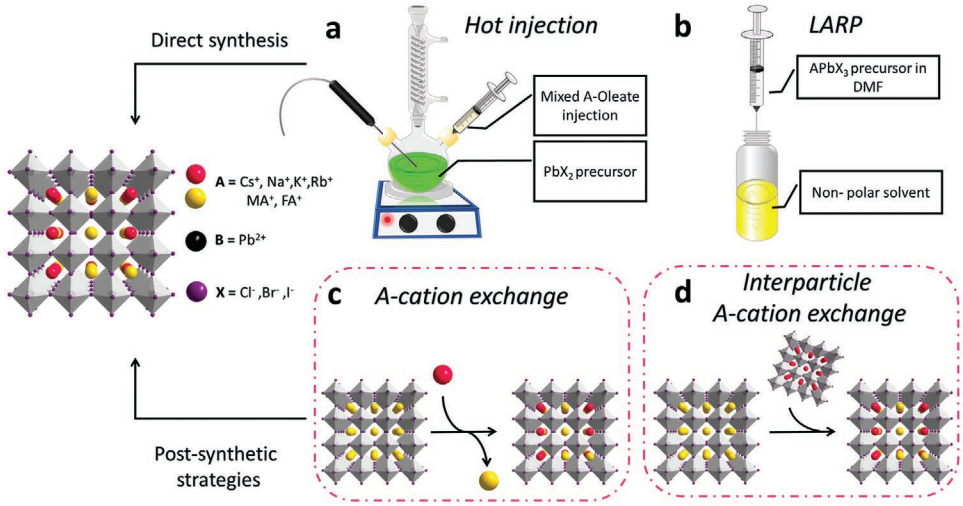

Figure 8. Synthesis methods to obtain mixed A-cation and Na^+, K^+, and Rb^+ cation LHP NCs. a,b) Direct synthesis of mixed cation LHP NCs by hot-injection (a) and ligand-assisted precipitation (b) approaches. In these methods, the corresponding A-cation precursors are mixed in the desired ratio to crystallize them into mixed-cation LHP NCs. c,d) Synthesis by post-synthetic A-cation exchange (c) and interparticle cross-exchange (d). In the cation exchange, some of the A-cations of pre-synthesized LHP NCs are exchanged with another A-cation using the corresponding precursor, for example, using A-oleate. In the interparticle cross-exchange process, two or more types of colloidal LHP NCs made of different A-cations are mixed to obtain a homogeneous solution of mixed A-cation LHP NCs through cross-exchange of A-cations. These strategies are also applicable to synthesize mixed A-cation and mixed halide perovskite NCs.

mixed A-cation and Na^+, K^+, and Rb^+ doped/alloyed mixed monovalent-cation perovskite NCs synthesized by different strategies.

The mixed A-cation LHP NCs can be synthesized directly using the mixture of desired A-cation precursors or by applying post-synthetic A-cation exchange and cross-exchange on pre-synthesized mono-cation LHP NCs, as illustrated in **Figure 8**. The direct synthesis can be carried out by classical methods such as hot-injection[48–175] or reprecipitation[49–177] (Figure 8a,b). In the hot-injection approach, the mixed cation LHP NCs are synthesized by injection of a mixture of one or more A-cation precursors into PbX_2-ligand solution at a high reaction temperature (Figure 8a). In the LARP approach, a DMF solution containing a mixture of different A-cation and PbX_2 precursors along with ligands is added to an antisolvent such as toluene to crystallize mixed cation LHP NCs (Figure 8b). The hot-injection synthesis approach has been greatly exploited to obtain Na^+, K^+, and Rb^+ doped/alloyed mixed monovalent-cation perovskite NCs,[169,11,29,163,170,178–180] but rarely used for Cs^+, MA^+, and FA^+ based mixed A-cation LHP NCs[59] (see Table 2). This is because the crystallization temperature for inorganic and organic A-cations can be different, leading to polydisperse samples. However, in the case of Na^+, K^+, and Rb^+ doping/alloying, these cations are most likely occupying the interstitial sites rather than the A-site of the perovskite lattice. On the other hand, the reprecipitation approach has been successfully applied to synthesize different types of mixed cation LHP NCs as most of the A-cations precursors crystallize at room temperature upon adding them to antisolvent (see Table 2). For example, Chem et al.[192] demonstrated the synthesis of $Cs_{1-m}FA_mPbBr_3$ NCs by reprecipitation of the corresponding precursors ($PbBr_2$, CsBr, and FABr dissolved in DMF) in toluene. They found that the Cs/FA alloy LHP NCs exhibit superior structural stability and higher PLQY compared to individual counterparts. The reprecipitation approach has been extended to mixed A-cation NCs of $Cs_{1-m}MA_mPbBr_3$,[161] $Cs_{1-m}FA_mPbBr_3$,[173,181] and $FA_{1-m}MA_mPbBr_3$.[171,172] Despite successful demonstration of the synthesis of mixed A-cation LHP NCs by hot-injection and reprecipitation, obtaining NCs with precise tunability of the A-cation composition with high degree of homogeneity is still challenging. This is because different A-cations crystalize under different reaction conditions, which makes it difficult to obtain both the desired composition and a uniform size distribution in the mixed A-cation LHP NCs.

In this regard, post-synthetic ion-exchange reactions have proven to be a good alternative to precise tunability of the composition of LHP NCs. Generally, ion exchange reactions provide access to materials that are difficult to obtain by direct synthesis methods. For instance, halide ion exchange as well as interparticle cross-exchange reactions have been largely exploited to precisely tune the emission color of LHP NCs. In principle, such reactions are also applicable to tune the A-cation composition of perovskite NCs, as illustrated in Figure 8c,d. In the A-site cation exchange reaction, colloidal LHP NCs of single A-cation are synthesized and after their purification and redispersion in a non-polar solvent, a source of a different A-cation is added to partially displace the first one in the crystal lattice (Figure 8c).[59] On the other hand, the mixing of LHP NCs made of different A-cations leads to an interparticle A-cation exchange, resulting in the formation of mixed A-cation LHP NCs (Figure 8d).[47] These reactions are analogous to those of halide exchange reactions on LHP NCs that are initially reported by Nedelcu et al.[182] and Akkerman et al.[63] However, the A-cation exchange in LHP NCs has been relatively less investigated compared to halide exchange. Akkerman et al. first noticed the sign of A-site cation exchange in LHP NCs during the study of halide exchange in $CsPbX_3$ NCs using methylammonium halides (MA-X) as halide source. The addition of methylammonium bromide salt to $CsPbBr_3$ NCs leads to a PL peak shift from 2.43 to 2.36 eV

due to the replacement of Cs^+ with MA^+ ions.[63] Later, Protesescu et al. demonstrated the synthesis of $Cs_{1-m}FA_mPbI_3$ with tunable Cs/FA composition through A-cation exchange using FA-OL and Cs-OL as the source of cations.[59] They have shown that the bandgap of Cs/FA alloy perovskite NCs is tunable in between their individual counterparts by changing the A-cation composition.

In addition, recent studies have demonstrated the preparation of mixed-cation LHP NCs through A-cation cross-exchange between NCs made of two different A-cations. For instance, Luther and co-workers demonstrated the cross-exchange of Cs^+ and FA^+ ions upon mixing the colloidal NCs of $CsPbI_3$ and $FAPbI_3$, leading to the formation of $Cs_{1-x}FA_xPbI_3$ alloy NCs (**Figure 9**a).[47] The GTF calculations suggest that all CA/FA compositions exhibit a stable perovskite phase (Figure 9b). The composition of Cs/FA and thus the bandgap of the alloy NCs is tunable in between their individual counterparts by varying the concentrations of the individual components that are mixed (Figure 9c). The alloying of A-cation can be probed by monitoring the PL spectra of the resultant mixture.[47,60,61,160] As the exchange takes place, the two PL peaks corresponding to the individual components merge into a single one, confirming the completion of the cation exchange (Figure 9d). The PL kinetics of the resulting mixture revealed that the cation cross-exchange is rather slow in well-purified NCs (almost no exchange takes place at room temperature), as it needs ≈22 h for the complete exchange at 45 °C. Nevertheless, the exchange rate increases by increasing the reaction temperature, as it completes in 60 min at 90 °C. The activation energy for the cross-exchange of Cs^+ and FA^+ in a mixture of $CsPbI_3$ and $FAPbI_3$ colloidal NCs was measured as ≈0.65 eV, which is higher than that reported for halide exchange in LHPs. Later, Hao et al.[61] found that the residual oleic acid ligands in the colloidal NCs suspensions can significantly lower the activation energy of the A-cation cross-exchange, and thus the cross-exchange completes in 30 min in the NCs purified only once, while it needs 24 h in the case of NCs purified twice. The free oleic acid molecules present in the colloidal solution act as transporters in the cross-exchange. Interestingly, the authors proposed that the cations segregate into small $FAPbI_3$ and $CsPbI_3$ domains in the crystal lattice. It is well known that the halide ions in the perovskite lattice segregate upon light illumination. In fact, the phase segregation has also been observed in Rb doped $CsPbBr_3$ NCs.[176] However, it is interesting that the A-cations (especially, FA and Cs) segregate without any external stress, and therefore this needs an in-depth investigation.

In principle, the mixing of different A-cations in the LHP NC lattice can also be probed by TCSPC measurements. It has been well studied that the excited state decay of FA-based LHP NCs is much slower compared to inorganic LHP NCs.[47] Therefore, the Cs/FA mixed cation LHPs exhibit intermediate PL decay time as compared to their individual counterparts, and the relaxation time becomes faster with increasing the Cs/FA ratio.[61] Similarly, the mixed cation LHP NCs exhibit XRD peaks centered in between their individual counterparts due to the difference in lattice constant.[47,61] Vigil et al. had a close look at the change in the crystal phase of the $FAPbI_3$ LHP NCs after A-site cation exchange with Cs^+. The incorporation of new A-cations in the lattice will contract or expand the lattice parameter (depending on the respective size of the cations), and thus affect the tilt of $[PbX_6]^{4-}$ octahedra of the crystal structure. It was found that the structural symmetry of $Cs_xFA_{1-x}PbI_3$

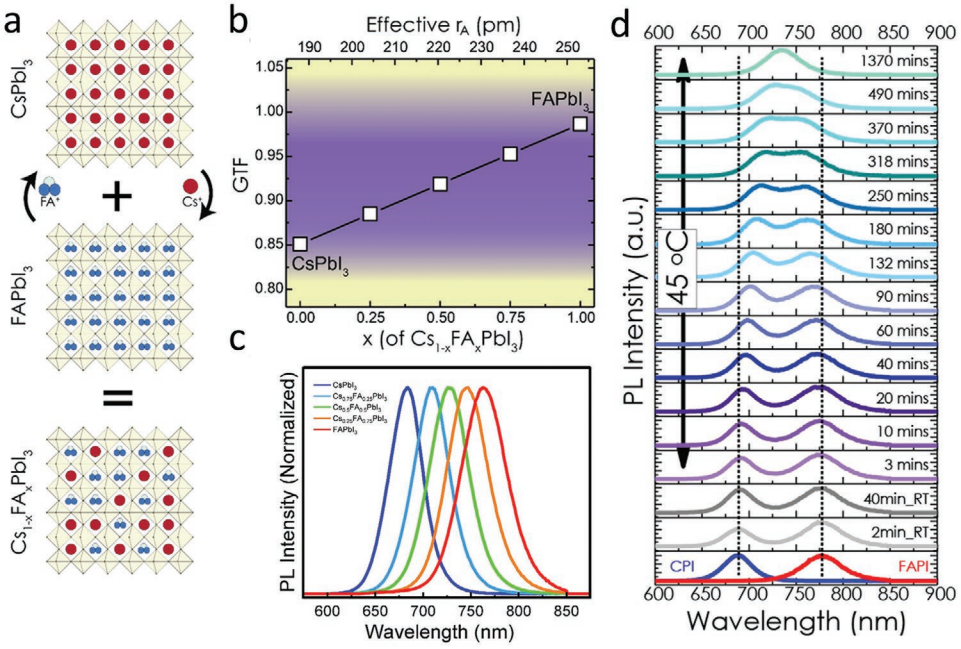

Figure 9. A-cation cross-exchange: a) Schematic illustration of cross-exchange of Cs^+ and FA^+ in between $CsPbI_3$ and $FAPbI_3$ NCs. b) A plot of the GTF versus [FA^+] concentration. The plot shows that all Cs/FA compositions are within the phase-stable region (purple). The top axis is the effective or average radius of A-cation. c) PL spectra of colloidal solutions of $CsPbI_3$, $FAPbI_3$, and $Cs_{1-x}FA_xPbI_3$ NCs of different Cs/FA ratios. d) Kinetic of A-site cation cross-exchange: time-dependent PL spectra of $CsPbI_3$ (CPI) and $FAPbI_3$ (FPI) colloidal NCs upon mixing them at 45 °C. Panels (a–d) are reproduced with permission.[47] Copyright 2018, American Chemical Society.

NCs is lowered from the α phase (cubic) to β (tetragonal) to γ (orthorhombic) phases with decreasing Cs content.[60] These studies need to be extended to other cation and halide compositions for a better understanding of the symmetry changes in mixed A-cation mixed halide systems.[19,34] Furthermore, the simultaneous cross-exchange of A-cation, as well as halide ion, leads to the formation of mixed cation mixed halide LHP NCs with tunable emission across the visible range.[160]

4.2. Mixed A-Cation LHP NC-Based Solar Cells

Despite the great success of LHP thin films as photosensitizers in highly efficient photovoltaics, achieving long-term stability while maintaining high efficiency is still challenging. Over the years, various approaches have been developed to improve their long-term phase stability.[6,187,188] Recently, the use of ligand-protected colloidal LHP NCs, especially $CsPbI_3$ and $FAPbI_3$ NCs, as photosensitizers has received increasing attention in the fabrication of PSCs with improved stability under long-term device operation.[14,47,61,62,160,189–194] Importantly, it has been found that the LHP NC-based solar cells exhibit higher open-circuit voltage (V_{OC}) compared to their thin-film photovoltaics.[61,195] This was attributed to the reduced non-radiative recombination in perovskite NC solar cells and thus leading to smaller V_{OC} losses relative to their bulk counterparts. The reduced non-radiative recombination is generally evident from the higher PLQY of LHP NC films compared to bulk thin-film perovskites. In addition, the capping ligands are expected to improve the intrinsic stability of the photoactive phase of iodide-based LHP NCs as compared with thin-film counterparts. The ligands can improve the stability against moisture. It is important to note that colloidal NCs need to be purified using antisolvents to remove the excess ligands in the solution as well as to reduce the ligand density on the NC surface, otherwise they can significantly reduce the device performance by blocking charge transport. However, the purification could lead to degradation and phase transformation of LHP NCs. As discussed in the earlier section, mixed A-cation LHP NCs exhibit higher phase stability and charge transport properties compared to their individual NCs. This is because the formation of mixed A-cation alloy in the crystal lattices favors the desired g tolerance factor for the stabilization of the perovskite structure under ambient conditions.[196] Furthermore, the fast rotation of FA in perovskite lattice results in enhanced orbital overlap and facile polaron formation, and thus leads to reduced non-radiative recombination and longer carrier lifetimes. Therefore, improving phase stability by A-cation engineering is desired as discussed in earlier sections. Recent studies have shown that the use of mixed A- cation LHP NCs as photosensitizers improves the long-term stability of perovskite photovoltaics while achieving over 10–15% PCE.[47,61,160,189,197] **Table 3** summarizes the recent literature on the mixed A-cation perovskite NC-based solar cells. It includes the device architecture, A-cation composition, and PCE. In 2018, Luther and co-workers demonstrated the fabrication of $Cs_{1-x}FA_xPbI_3$ NC-based solar cells that exhibit stable power out efficiencies with low hysteresis.[47] More importantly, the mixed cation NCs exhibit greater stability as compared with hybrid perovskites, as discussed in the previous section. Furthermore, they found that the V_{OC} increases with increasing the Cs content in the NCs. However, the NC-based solar cells possess higher V_{OC} compared to the bulk photovoltaics regardless of their A-cation composition. In 2020, Hao et al.[61] reported over 15% PEC using $Cs_{1-x}FA_xPbI_3$ NCs and SnO_2 layer interface between ITO and the NC layer (**Figure 10**a,b). They found that the mixed cation- solar cells exhibit higher PCE compared to $CsPbI_3$ NC solar cells. More importantly, the mixed NC solar cells showed suppressed phase segregation and long-term stability for device operation under continuous illumination of 1-sun. On the other hand, few studies have been focused on the integration of mixed cation NCs into bulk thin-film photovoltaics to improve their stability. For instance, Ou Chen and co-workers demonstrated that the use of Cs rich mixed cation $Cs_{1-x}FA_xPbI_3$ NC layer on top of bulk $FAPbI_3$ layer improves the stability of the device under ambient conditions while maintaining over 19% PCE (Figure 10c–e).[189] The device shows negligible hysteresis compared to the device without the NC layer (Figure 10d). They found that the NC layer integrated $FAPbI_3$ solar cell device exhibited significantly improved stability compared to the device without NCs layer under 90% relative humidity. These studies clearly demonstrate the potentiality of mixed cation NC systems for improving the stability of PSCs. However, the device efficiency is relatively low compared to bulk thin film-based solar cells. Therefore, the future focus should be on improving the efficiency of mixed A-cation NC photovoltaics by optimizing the interfaces (electron and hole-transport layers).

5. Mixed A-Site Cation Perovskites for LEDs (Bulk Thin-Films and NCs)

As can be seen from earlier sections, LHPs are one of the leading candidates for the next generation of optoelectronic

Table 3. Literature overview of mixed A-cation NC solar cells made of different NC compositions, device architectures, and obtained PCE.

Composition	Year	Device architecture	PCE	Ref.
$Cs_{0.75}FA_{0.25}PbI_3$ QDs	2018	Al/MoO_x/Spiro-OMeTAD/QDs/TiO_2/FTO	11.14	[47]
$Cs_{1-x}FA_xPbI_3$ QDs	2019	Al/MoO_3/PTTA/$FAPbI_3$ QDs/$CsPbI_3$ QDs/TiO_2/FTO	15.6	[197]
$FA_{0.55}Cs_{0.45}Pb(I_{0.55}Br_{0.45})_3$ QDs	2019	Al/MoO_x/Spiro-OMeTAD/QDs/TiO_2/FTO	9.86	[160]
$CsPbI_3$:$Cs_{0.25}FA_{0.75}PbI_3$ QDs	2019	Al/MoO_x/Spiro-OMeTAD/QDs/TiO_2/ITO	17.39	[192]
$FAPbI_3$ thin film:$Cs_{0.57}FA_{0.43}PbI_3$ QDs	2019	Au/Spiro-OMeTAD/$Cs_{0.57}FA_{0.43}PbI_3$ QDs/$FAPbI_3$ thin film/SnO_2/FTO	20.82	[189]
$Cs_{0.5}FA_{0.5}PbI_3$ QDs	2020	Au/Spiro-OMeTAD/QDs/SnO_2/ITO	16.6	[61]
$(FAPbI_3)_x(MAPbBr_3)_{1-x}$ thin film: $Cs_{0.05}(FA_{0.83}MA_{0.17})_{0.95}PbBr_3$ QDs	2020	Au/Spiro-OMeTAD/QDs/SnO_2/FTO	21.10	[198]
$Cs_{1-x}FA_xPbI_3$ QDs	2020	Au/Spiro-OMeTAD/$CsPbI_3$ QDs/$FAPbI_3$ QDs/SnO_2/FTO	16.07	[199]

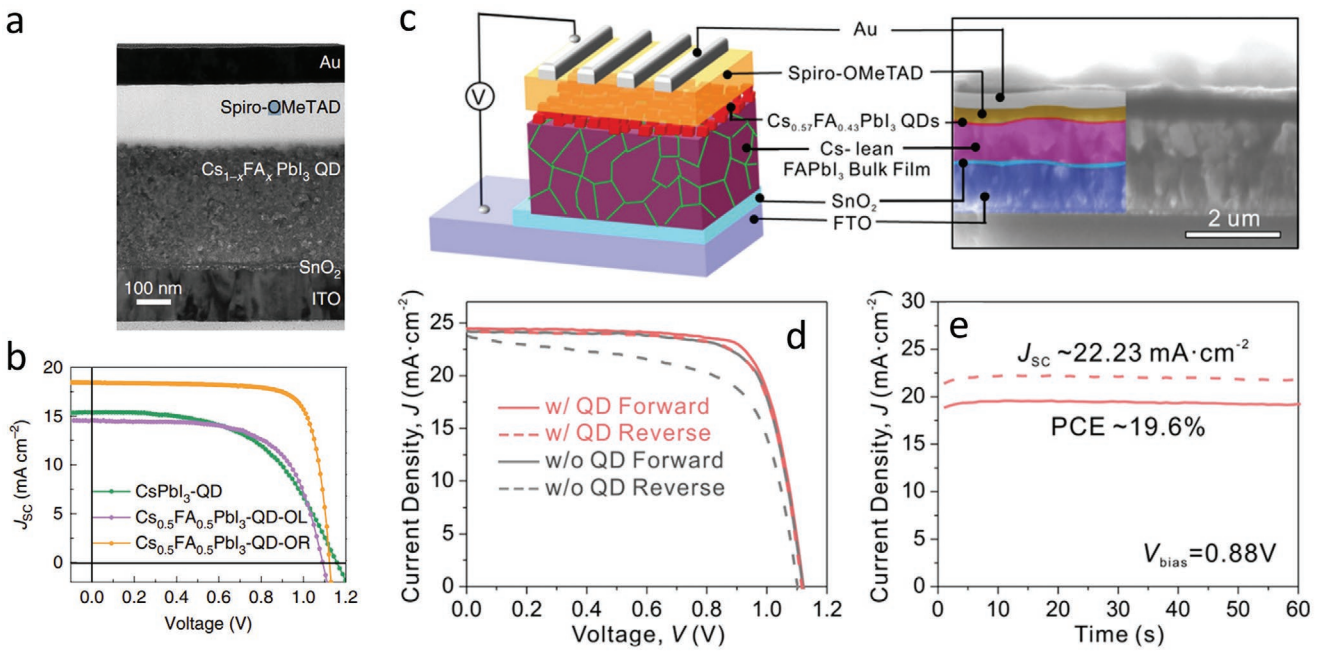

Figure 10. a) Cross-section SEM image of the $Cs_{1-x}FA_xPbI_3$ NC solar cells. b) *J–V* characteristics of the solar cells made of different NCs as photosensitizers. Panels a and b are reproduced from Ref. [61]. Copyright 2020, Springer Nature. c) Schematic illustration of the device architecture and the cross-section SEM image of the real device made of $FAPbI_3$ bulk film and $Cs_{1-x}FA_xPbI_3$ NC layers. d) *J–V* (forward and reverse) characteristics of the solar devices with and without $Cs_{1-x}FA_xPbI_3$ NC layer. e) Photocurrent density and PCE output characteristics at the maximum power point ($V = 0.88$ V). Panels (c) and (d) are reproduced from Ref. [189]. Copyright 2019, American Chemical Society.

applications, including light emission.[14,200,201] Compositional engineering[202] and dimensional engineering[203] are widely used to tune the optoelectronic properties of halide perovskites. In this section, we will focus on A-site compositional engineering, and discuss the effects on LED device performance.

The importance of mixed A-site cations on LED device performance has been studied by many groups, as summarized in **Table** 4. Many studies have shown that by having multiple cations at A-site such as FA, MA, or Cs, the external quantum efficiency (EQE) of LED is higher than in mono-cation perovskite LEDs.[14,173,204–207] For example, Zhang et al. conducted a systematic investigation into the effect of mixing FA and Cs on the performance of perovskite LEDs.[173] The study showed that alloying up to 20% Cs influenced the perovskite crystal lattice and improved the device performance from maximum luminance of 8563 cd m^{-2} and EQE of 0.82% for neat $FAPbBr_3$ LEDs to 55 005 cd m^{-2} and 2.8% for $FA_{0.8}Cs_{0.2}PbBr_3$ LEDs.[173] Similarly, Xie et al. demonstrated that by preparing mixed cations thin films ($Cs_{0.76}FA_{0.24}PbBr_3$), the operational stability and initial maximum luminance of the LEDs can be increased over $CsPbBr_3$ emitters.[207] In **Figure 11**, the current understanding of the mechanisms behind the improvement in device performance with A-site cation alloying is discussed. Figure 11a shows that the mixed cation films show slower PL decay than the pure Cs-cation films. The time-resolved PL (TRPL) decay curves were fitted with a tri-exponential decay model. The short, intermediate, and long-time constants obtained from fitting with this model were denoted τ_1, τ_2, and τ_3, respectively, as shown in Figure 11b. Typically, the short and intermediate lifetime components (τ_1 and τ_2) were ascribed to two types of trap-assisted recombination (surface and bulk), whereas the long lifetime component (τ_3) was ascribed to intrinsic trap-free charge recombination.[208,209] However, we note that such a simple model may deviate from the underlying physical processes in the films. The tri-exponential model nevertheless provides a useful numerical description of the TRPL decay curves that can be used for comparisons. The total proportion of τ_1 and τ_2 in the CsFA film was significantly lower than that in the Cs film (Figure 11b), indicating that fewer traps participated in the PL decay processes. The alloying of FA into Cs improved the film morphology during crystallization which increased the device efficiency. Additionally, the intrinsic excitonic binding energy was increased to 59.2 meV for mixed cation films, which was higher than those of both the pure FA (25 meV) and pure Cs (37 meV) cation monocrystalline films.[207] The higher exciton binding energy in mixed cation perovskite films could have led to an increase in the intrinsic PLQY, thus improving the device efficiency.[6,210,211]

Mixing the species present at the A-site can also influence the crystalline phase of the perovskite emitters. Liu et al. concluded that the use of a mixture of A-site cations significantly influences the crystallization of the perovskite films.[218] Their DFT calculations (Figure 11d,e) demonstrated that different A-site cations can lead to different phases. For example, pure FA led to a cubic phase and pure Cs led to an orthorhombic phase, while using a mixture of both ($Cs_{0.5}FA_{0.5}PbBr_3$) led to a tetragonal phase.[218] It was found that tetragonal $Cs_{0.5}FA_{0.5}PbBr_3$ was slightly more stable than the cubic structures. They showed that perovskite thin films with a 1:1 mixture of Cs and FA cations were comprised of small crystals in a disordered matrix that may passivate the surface defects and improve the radiative efficiency, thus improving device performance. However, more

Table 4. Literature overview of mixed A-cation NC LEDs made of different compositions, device architectures, emission wavelength together with full width half maximum, luminescence intensity, turn-on voltage, and obtained EQE.

Emitting layer	Device structure	EL λ_{max}(FWHM)/[nm]	EQE_{max} [%]	L_{max}[cd m^{-2}]	Voltage [V]	Year/ref.
Nanocrystals						
$MA_{0.7}Cs_{0.3}PbBr_3$ NCs	ITO/PEDOT:PSS/TFB/Pero/TPBi/LiF/Al	520 (25)	1.3	24 500	4	2017[161]
$Cs_x(MA_{0.17}FA_{0.83})_{1-x}PbBr_3$ NCs	ITO/PEDOT:PSS/Poly-TPD/Pero/POT-2T/LiF/Al	523 (19)	7.36	10 207	2	2020[162]
$Cs_yGA_{1-y}PbBr_xCl_{3-x}$	ITO/PEDOT:PSS/PTAA/Pero/TPBi/LiF/Al	490 (18)	3.02	603	2.6	2021[215]
$Cs_yFA_{1-y}PbBr_xCl_{3-x}$	ITO/PEDOT:PSS/PTAA/Pero/TPBi/LiF/Al	492 (18)	4.14	1762	2.7	2021[215]
Thin Films						
$Cs_xFAyRb_{1-x-y}PbBr_zCl_{3-z}$	ITO/NiO_x/PVK/PVP/Pero/TPBi/LiF/Al	477 (18)	11	2180	2.6	2021[219]
$Cs_{0.76}FA_{0.24}PbBr_3$	ITO/ZnO/PVA/TFB/Pero/PVK/MoO_3/Al	518 (20)	3.8	72 763	2.6	2019[207]
$FA_{0.8}Cs_{0.2}PbBr_3$	ITO/PEDOT:PSS/TFB/Pero/TPBi/LiF/Al	527 (23)	2.8	55 005	3.5	2017[173]
$Cs_x(MA_{0.17}FA_{0.83})Pb(I_{0.83}Br_{0.17})_3$	ITO/PEDOT:PSS/Pero/F8/MoO_3/Ag	750	5.9	986	3	2022[205]
$Cs_{10}(MA_{0.17}FA_{0.83})Pb(Br_xI_{1-x})_3$	ITO/AZO/AZO:Cs/Pero/CuS-GaSnO/WO3/Au	569 (27)	12.98	55 370	2.5	2018[220]
$FA_{1-x}Cs_xPbBr_3$	ITO/SOCP/MHP/TPBI/LiF/Al	541 (24)	3.1	9834	3.6	2018[204]
$FA_{0.93}Rb_{0.07}PbBr_3$	ITO/PEDOT:PSS/Perovskite/TPBi/LiF/Al	532	7.2	66 353		2018[213]
$MA_{(1-x)}Rb_xPbBr_3$	ITO/PEDOT:PSS/Perovskite/TPBi/LiF/Al	526 (18)		7694	3	2018[212]
$MA_xEA_{(1-x)}PbBr_3$	ITO/PEDOT:PSS/Perovskite:PEABr/TmPyPB/CsF/Al	515 (21)	14.5	13 900	2.7	2020[214]
$Cs_{0.5}FA_{0.5}PbBr_3$	ITO/NiO_x/TFB/Pero/TPBi/LiF/Al	526	12.1	15 070		2021[206]

studies are needed to fully understand the relation between the composition at the A-site and the phases present. Further discussions on this topic based on bulk samples are given earlier in Section 3.

We would like to emphasize the role of interactions between organic A-site molecules and the inorganic Pb-halide (Pb-X) framework (Figure 11g). Zhang et al. demonstrated that by adding small quantity of GA or FA into $CsPbBr_xCl_{3-x}$ perovskite quantum dots, the EQE and spectral stability of the devices were improved.[14] The mechanism behind this improvement is attributed to the strong hydrogen bonding between the amine group and halide in the inorganic octahedra, thereby increasing the energy barrier for halide anion migration, thereby reducing halide segregation and stabilizing the electroluminescence spectra (see Section 3.1 and 3.2 for further discussions on this topic). Their calculations showed that the energy barrier for halides to migrate can be increased from 0.42 eV (pure Cs) to 0.49 eV (with GA) or 0.52 eV (with FA) (Figure 11h). As a result, the EQE increased from 1.3% ($CsPbBr_xCl_{3-x}$) to 3.02% ($GACsPbBr_xCl_{3-x}$) and 4.14% ($FACsPbBr_xCl_{3-x}$) with more stable EL spectra.[215]

Apart from commonly studied A-site cations like Cs^+, FA^+, and MA^+, other functional A-site cations have also been investigated for PeLEDs.[212–214] Rubidium cations can also fit inside the cuboctahedral voids in the perovskite framework. Binyamin et al reported a series of fully-inorganic mixed Cs-Rb cation LHP NCs, $Cs_xRb_{1-x}PbBr_3$ (x = 0–0.8).[176] Incorporation of the smaller Rb^+ (x = 0.2) can reduce the FWHM of the PL peak from 17.7 to 17.0 nm. Also, they observed the formation of core-shell structures when the concentration of the Rb precursor in the starting solution was increased. Rb ions have also been added to MA-based and FA-based perovskite thin films to improve the efficiency. For example, Kanwat et al. reported that by adding Rb^+ to $MAPbBr_3$ thin films with 1:1 mole ratio, the maximum luminance can be improved from 754 to 7694 cd m^{-2} and current efficiency increased from 0.49 to 9.45 cd A^{-1}.[177] Similarly, Shi et al. reported an increase in EQE from 1.47% to 7.17% when doping 30% Rb into $FAPbBr_3$ films.[213] These improvements were attributed to a reduction in the defect density and hence suppressed non-radiative recombination.[212–213] However, more studies are required to fully understand the role of mixed A-site cations on improving the optical properties of the films. For example, Feldmann et al demonstrated that mixing cations would create spatially-varying energetic disorder in the electronic states, leading to local charge accumulation, creating p- and n-type photodoped regions.[227] The carriers would then localize to the low bandgap regimes caused by cation tailoring. These photodoping areas have higher luminescence yields which originate from radiative rates outcompeting non-radiative losses, since carrier densities remain locally high in these charge-accumulation regions.

Amine-based cations apart from FA and MA are another interesting group of A-site cations that have been explored. For example, Xiao et al. mixed methylammonium (MA) and ethylammonium (EA) cations and fabricated $MA_xEA_{(1-x)}PbBr_3$ PeLED.[214] The EQE increased from 4.1% for single cation ($MAPbBr_3$) PeLEDs to 14.5% (MA:EA in a 2:1 molar ratio). Based on their XRD analysis, the addition of EA cations did not disrupt the crystal structure of the perovskites, but only shifted the XRD peak positions to lower 2θ values.[226] Similarly, the incorporation of guanidine ions into $CsPbBr_xCl_{3-x}$ reported by Zhang et al did not alter the phase of the films.[215] However, when the A-site cations were large enough to no longer fit into the cuboctahedral voids in the perovskite, such as

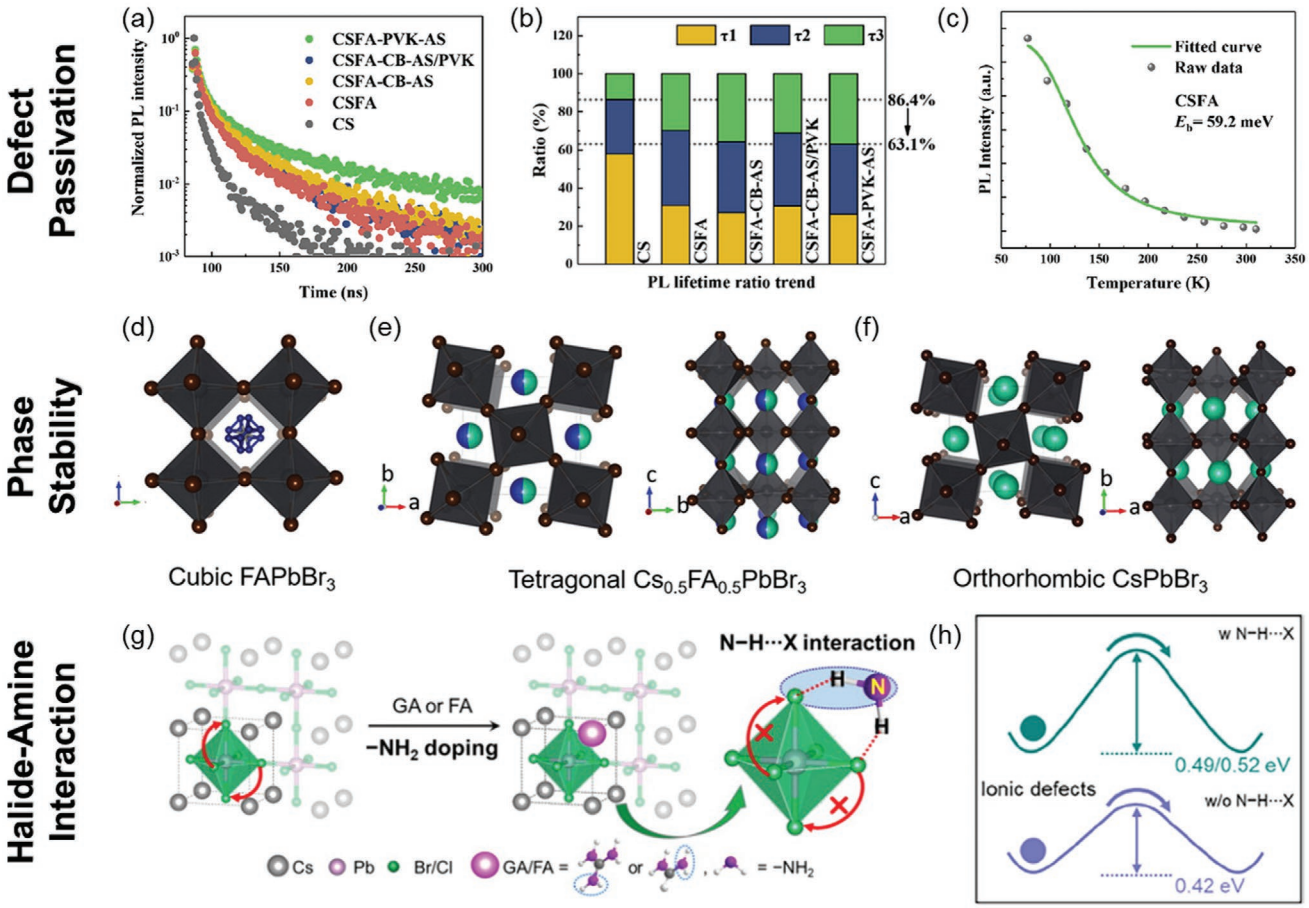

Figure 11. The effect of cation mixing on LEDs device performance. Mixed cations passivate defects. a) TRPL decay for pure $CsPbBr_3$ film (Cs), $Cs_xFA_{1-x}PbBr_3$ film, $Cs_xFA_{1-x}PbBr_3$ films treated with chlorobenzene antisolvents (CB-AS) and/or Poly(9-vinylcarbazole) (PVK) antisolvents (PVK-AS). b) The TRPL decay constant ratio. c) Fitted curve of the temperature-dependent PL intensity of the $Cs_xFA_{1-x}PbBr_3$ film. (Exciton binding energy (Eb) can be extracted.) The figures are reproduced with permission.[207] Copyright 2019, Elsevier B.V. Mixed cations influence perovskite phase transformation during crystallization. (d–f) shows different calculated phases including cubic phase for pure $FAPbBr_3$, tetragonal phase for mixed Cs-FA, and orthorhombic phase for pure $CsPbBr_3$. The figures are reproduced with permission.[206] Copyright 2021, Wiley-VCH GmbH. Organic–inorganic mixed cations induce stronger halide-cation interaction through H-bonding between halides and amines. g) Schematic of inhibiting ion migration for $CsPbBr_xCl_{3-x}$ QDs by N-H–X doping strategy. Doped cations containing -NH_2 are introduced into the perovskite crystal lattice, N-H–X H-bonds are formed between the N-H dopants and Pb-X lattices, which can inhibit the migration of halide ions, thereby stabilizing the color-shift. h) Schematic of the energy barrier for ionic migration dependence on N-H–X interactions. The figures are reproduced with permission.[215] Copyright 2021, Science China Press. Published by Elsevier B.V. and Science China Press.

phenethylammonium ions (PEA^+), the bulky cations would cut the bulk 3D structure into quantum-confined 2D structures or quasi-2D structures. The progress of quasi-2D PeLED is beyond the scope of this review. Recent reviews on this topic can be found in Ref. [216–218].

6. Summary and Outlook

6.1. Mixed A-Cation Thin-film Solar Cells

Organic–inorganic hybrid perovskites have emerged over the last decade as exceptional optoelectronic materials for a wide range of applications, due to their long charge-carrier diffusion lengths, high absorption coefficients, low exciton binding energies (in bulk materials), and high radiative efficiencies. Uniquely, these properties are achieved in materials processed with low-temperature solution-based methods, which arise in part from the defect tolerance of the materials. By optimizing different parts of PSC devices, such as charge transport layers, interface, and film morphology, as well as through defect passivation, the PCE has reached up to a certified value of 25.7%. In particular, the possibility of perovskite compositional engineering provides an excellent opportunity to design desirable bandgaps to absorb light from different spectral regions, facilitating the fabrication of multijunction solar cells. A-site cation engineering (i.e., forming multi-cation perovskites), could enhance the efficiency and stability of MA-, FA-, or Cs-based perovskites. We discussed all the possibilities of mixing the A-site cations, including double-, triple-, and quadruple perovskites, focusing on the phase stability and the fabrication of highly efficient solar cells. In brief, introducing

multication compositions with different ionic radii to occupy different positions in the perovskite crystals could modify the perovskite properties, leading to high-performance PSCs with record efficiency and stability. The increased stability is often attributed to the favorable GTF for the perovskite phase upon A-site alloying. It is well established that the A-site alloying improves the stability as well as reproducibility of PSCs. However, the relationship of chemical composition-crystal structure-property-performance-phase stability is yet to be established. To this end, machine-learning tools could be applied to unveil this relationship by high-throughput screening of reported experimental data.[221–222] In addition, it could be useful to identify the optimum composition, device structure, and fabrication parameters for reproducible and efficient solar cells. Nevertheless, the lack of detailed information about the crystallization mechanism and role of different cations in perovskite thin films needs to be urgently addressed. Over the years, various techniques (using standard XRD and grazing incidence X-ray scattering in small-angle or wide-angle configurations (GISAXS and GIWAXS), PL, and UV–vis absorption) have been developed for in situ monitoring of the nucleation of growth of grains in perovskite thin films.[223–227] Although these techniques have advanced our understanding of the nucleation and growth of perovskite films, the role of different A-cations in the growth process and their distribution in mixed A-cation perovskite lattice, and the structural heterogeneity across the film are yet to be explored. Therefore, novel techniques that combine the capabilities to simultaneously obtain optical and structural information of mixed A-cation perovskite systems. In addition, studying the formation of perovskite crystals through in situ liquid cell transmission electron microscopy techniques would be ideal to understand the growth mechanism as well as the role of different cations. However, this is extremely challenging due to the fast degradation of perovskites under electron beam.

6.2. Mixed A-Cation LHP Colloidal NCs

On the other hand, the A-site composition of colloidal LHP NCs is precisely controllable by post-synthetic cation exchange using corresponding cation precursors or cross-exchange between NCs of different A-site cations. Although the cation cross-exchange does not occur in well purified LHP NCs at room temperature, the excess ligands present in the impurified colloidal NCs significantly lower the activation energy of the exchange process and thus facilitate the cross-exchange. Importantly, it has been found that the mixed cation LHP NCs, for example, $Cs_xFA_{1-x}PbI_3$ NCs, exhibit higher phase stability over their pure counterparts. Consequently, the solar cells made of mixed-cation LHP NCs exhibit long-term stability while maintaining high PCE as high as the single A-site cation LHP NCs. In fact, the highest PCE of LHP NC solar cells reported until today is based on $Cs_xFA_{1-x}PbI_3$ NC photosensitizers (Table 3). Furthermore, it has been demonstrated that the integration of mixed cation NCs layer on top of bulk thin-film perovskite improves the device operational stability while achieving over 20% PCE. Despite decent progress in mixed cation LHP NC solar cells, there are several outstanding questions that need to be addressed in future studies. The toxicity of Pb is one of the major concerns for real-world applications of LHP NCs, therefore, Pb-free halide perovskites have received increasing attention. We have witnessed some progress in lead-free thin-film perovskites in the last 5 years. The knowledge generated from Pb-free thin-film PSC research can be used to obtain novel Pb-free colloidal halide perovskite NCs. Generally, some of the Pb-free halide perovskite NCs are relatively unstable and tend to degrade in a few hours after their preparation. Consequently, it would be interesting to investigate whether or not the A-site cation engineering improves the stability of perovskite NCs. Future research should therefore focus on the development of solar cells using Pb-free halide perovskite NCs as photosensitizers. Furthermore, it is important to scale up the PSCs (thin films as well as NCs-based) into module scale while maintaining high PCE. Therefore, future studies should be focused on the implementation of the A-site cation allying strategy to achieve module scale devices. In addition, the surface chemistry of perovskite NCs should be optimized to improve the device performance. The long-chain ligands on the surface of perovskite NCs hinder the charge transport between NCs of the corresponding thin films. Therefore, the ligand type and the density of ligands on NC's surface need to be optimized to improve carrier transport in NC films. However, the removal of ligands from the NC surface can cause the aggregation or degradation of NCs. To address this issue, novel purification methods need to be developed to obtain well-purified and stable colloidal NCs. Furthermore, the mixed cation perovskite NC systems can be integrated with other materials such as polymers, classical QDs to obtain hybrid systems to fabricate stable and efficient solar cells. More importantly, these systems need to be characterized by advanced spectroscopy techniques to understand the role of mixed A-site cations, charge carrier transport, distribution of cations, and phase stability.

6.3. Properties of Mixed A-Cation Perovskite Systems

Correlative characterization (especially nuclear magnetic resonance, nuclear quadrupole resonance, and neutron diffraction techniques), along with first-principles calculations, have been invaluable in elucidating the role of the size and shape of the A-site cation on the properties of halide perovskites. The re-orientational dynamics of the alkylammonium cation accessible at different temperatures determine the tilting of the inorganic octahedra, which in turn determines the structure and phase transitions possible. This has provided insights into the different structural transitions of MA- and FA-based perovskites, and how these are influenced by alloying the A-site cation with Cs. In-depth studies have particularly been invaluable to understand the importance of octahedral tilting in preventing the degradation of $FAPbI_3$ to the undesired hexagonal phase, as well as showing novel routes to maintain the photoactive a-phase through judicious choice of ligands to stabilize the tilting of octahedra. However, the understanding of the role of the re-orientation dynamics, dipole moment, quadrupole moment, size, and shape of the A-site cation on the phases formed by

the perovskites is still at an early stage. For example, there are disagreements into the influence of Cs alloying on the re-orientation dynamics of FA in FA-based lead-halides, and an understanding of how the A-site cation composition influences halide migration is also in the early stages. In-depth studies continuing on recent work will be important to unveil new strategies to improve the stability and performance of the hybrid halide perovskites.

6.4. Mixed A-Cation LHP NC LEDs

In general, double[14,161,204,206,207] and triple cation[162,205,219,220] perovskite emitters show higher performance and operational stability than single-cation perovskites. A variety of possible explanations have been put forward, including passivation effects, improvements in film crystallinity, and increased hydrogen bonding between the amine group of the alkylammonium cation and the halides from the inorganic octahedra. However, there are still many questions in the field. For example, the relationship between the composition of the A-site cation and device performance is not yet fully understood. The level of distortion of the octahedra upon tuning the fraction of inorganic versus organic species at the A-site needs to be studied in order to obtain compositions that give the optimal optoelectronic properties, such as high PLQY and low defect densities. Furthermore, the EQE of double- and triple-cation perovskite LEDs, and their operational stability, still need to be further improved by rational optimization of the composition at the A-site and X-site.

Acknowledgements

L.P. acknowledges the support from the Spanish Ministerio de Ciencia e Innovación through Ramón y Cajal grant (RYC2018-026103-I) and the Spanish State Research Agency (Grant No. PID2020-117371RA-I00), the grant from the Xunta de Galicia (ED431F2021/05). Funding from Xunta de Galicia/FEDER (grant GRC ED431C2020/09) is gratefully acknowledged. R.L.Z.H. would like to acknowledge support from the Royal Academy of Engineering under the Research Fellowships scheme (no.: RF\201718\1701). J.S. would like to acknowledge support from the DGIST Start-up Fund Program of the Ministry of Science and ICT (2021070009). M.S. thanks the German Research Foundation (DFG) for funding (SPP2196, 431314977/GRK 2642). M.M.B. thanks the Helmholtz Young Investigator Group FRONTRUNNER. M.S. acknowledges funding by ProperPhotoMile. Project ProperPhotoMile is supported under the umbrella of SOLAR-ERA.NET Cofund 2 by The Spanish Ministry of Science and Education and the AEI under the project PCI2020-112185 and CDTI project number IDI-20210171; the Federal Ministry for Economic Affairs and Energy on the basis of a decision by the German Bundestag project number FKZ 03EE1070B and FKZ 03EE1070A and the Israel Ministry of Energy with project number 220-11-031. SOLAR-ERA.NET is supported by the European Commission within the EU Framework Programme for Research and Innovation HORIZON 2020 (Cofound ERA-NET Action, No. 786483). The authors acknowledge the Universidade de Vigo/CISUG for open access funding.

Conflict of Interest

The authors declare no conflict of interest.

Keywords

lead-halide perovskites, light-emitting diodes, mixed cation perovskites, perovskite nanocrystals, photovoltaics, spectroscopy, synthesis

Received: February 22, 2022
Revised: May 3, 2022
Published online: June 22, 2022

[1] J. Burschka, N. Pellet, S.-J. Moon, R. Humphry-Baker, P. Gao, M. K. Nazeeruddin, M. Grätzel, *Nature* **2013**, *499*, 316.
[2] M. M. Byranvand, T. Kim, S. Song, G. Kang, S. U. Ryu, T. Park, *Adv. Energy Mater.* **2018**, *8*, 1702235.
[3] A. Kojima, K. Teshima, Y. Shirai, T. Miyasaka, *J. Am. Chem. Soc.* **2009**, *131*, 6050.
[4] S. D. Stranks, H. J. Snaith, *Nat. Nanotechnol.* **2015**, *10*, 391.
[5] Z.-K. Tan, R. S. Moghaddam, M. L. Lai, P. Docampo, R. Higler, F. Deschler, M. Price, A. Sadhanala, L. M. Pazos, D. Credgington, F. Hanusch, T. Bein, H. J. Snaith, R. H. Friend, *Nat. Nanotechnol.* **2014**, *9*, 687.
[6] J. Ye, M. M. Byranvand, C. O. Martínez, R. L. Z. Hoye, M. Saliba, L. Polavarapu, *Angew. Chem., Int. Ed.* **2021**, *60*, 21636.
[7] G. Xing, N. Mathews, S. S. Lim, N. Yantara, X. Liu, D. Sabba, M. Grätzel, S. Mhaisalkar, T. C. Sum, *Nat. Mater.* **2014**, *13*, 476.
[8] H. Wang, D. H. Kim, *Chem. Soc. Rev.* **2017**, *46*, 5204.
[9] Q. Chen, J. Wu, X. Ou, B. Huang, J. Almutlaq, A. A. Zhumekenov, X. Guan, S. Han, L. Liang, Z. Yi, J. Li, X. Xie, Y. Wang, Y. Li, D. Fan, D. B. L. Teh, A. H. All, O. F. Mohammed, O. M. Bakr, T. Wu, M. Bettinelli, H. Yang, W. Huang, X. Liu, *Nature* **2018**, *561*, 88.
[10] M. A. Green, A. Ho-Baillie, H. J. Snaith, *Nat. Photonics* **2014**, *8*, 506.
[11] Z. Saki, M. M. Byranvand, N. Taghavinia, M. Kedia, M. Saliba, *Energy Environ. Sci.* **2021**, *14*, 5690.
[12] M. Saliba, *Science* **2018**, *359*, 388.
[13] L. Schmidt-Mende, V. Dyakonov, S. Olthof, F. Ünlü, K. M. T. Lê, S. Mathur, A. D. Karabanov, D. C. Lupascu, L. M. Herz, A. Hinderhofer, F. Schreiber, A. Chernikov, D. A. Egger, O. Shargaieva, C. Cocchi, E. Unger, M. Saliba, M. M. Byranvand, M. Kroll, F. Nehm, K. Leo, A. Redinger, J. Höcker, T. Kirchartz, J. Warby, E. Gutierrez-Partida, D. Neher, M. Stolterfoht, U. Würfel, M. Unmüssig, et al., *APL Mater.* **2021**, *9*, 109202.
[14] A. Dey, J. Ye, A. De, E. Debroye, S. K. Ha, E. Bladt, A. S. Kshirsagar, Z. Wang, J. Yin, Y. Wang, L. N. Quan, F. Yan, M. Gao, X. Li, J. Shamsi, T. Debnath, M. Cao, M. A. Scheel, S. Kumar, J. A. Steele, M. Gerhard, L. Chouhan, K. Xu, X.-g. Wu, Y. Li, Y. Zhang, A. Dutta, C. Han, I. Vincon, A. L. Rogach, et al., *ACS Nano* **2021**, *15*, 10775.
[15] H. Min, D. Y. Lee, J. Kim, G. Kim, K. S. Lee, J. Kim, M. J. Paik, Y. K. Kim, K. S. Kim, M. G. Kim, T. J. Shin, S. Il Seok, *Nature* **2021**, *598*, 444.
[16] J. J. Yoo, G. Seo, M. R. Chua, T. G. Park, Y. Lu, F. Rotermund, Y.-K. Kim, C. S. Moon, N. J. Jeon, J.-P. Correa-Baena, V. Bulović, S. S. Shin, M. G. Bawendi, J. Seo, *Nature* **2021**, *590*, 587.
[17] Z. Liang, S. Zhao, Z. Xu, B. Qiao, P. Song, D. Gao, X. Xu, *ACS Appl. Mater. Interfaces* **2016**, *8*, 28824.
[18] T. Jesper Jacobsson, J.-P. Correa-Baena, M. Pazoki, M. Saliba, K. Schenk, M. Grätzel, A. Hagfeldt, *Energy Environ. Sci.* **2016**, *9*, 1706.
[19] H. Min, M. Kim, S.-U. Lee, H. Kim, G. Kim, K. Choi, J. H. Lee, S. I. Seok, *Science* **2019**, *366*, 749.
[20] J. J. Yoo, S. Wieghold, M. C. Sponseller, M. R. Chua, S. N. Bertram, N. T. P. Hartono, J. S. Tresback, E. C. Hansen, J.-P. Correa-Baena, V. Bulović, T. Buonassisi, S. S. Shin, M. G. Bawendi, *Energy Environ. Sci.* **2019**, *12*, 2192.

[21] B. O'Regan, M. Grätzel, *Nature* **1991**, *353*, 737.
[22] N. Gasparini, A. Salleo, I. McCulloch, D. Baran, *Nat. Rev. Mater.* **2019**, *4*, 229.
[23] Y.-W. Su, S.-C. Lan, K.-H. Wei, *Mater. Today* **2012**, *15*, 554.
[24] G. H. Carey, A. L. Abdelhady, Z. Ning, S. M. Thon, O. M. Bakr, E. H. Sargent, *Chem. Rev.* **2015**, *115*, 12732.
[25] National Renewable Energy Laboratory Best Research-Cell Efficiency Chart, (accessed: January 2022).
[26] A. Al-Ashouri, E. Köhnen, B. Li, A. Magomedov, H. Hempel, P. Caprioglio, J. A. Márquez, A. B. M. Vilches, E. Kasparavicius, J. A. Smith, N. Phung, D. Menzel, M. Grischek, L. Kegelmann, D. Skroblin, C. Gollwitzer, T. Malinauskas, M. Jošt, G. Matič, B. Rech, R. Schlatmann, M. Topič, L. Korte, A. Abate, B. Stannowski, D. Neher, M. Stolterfoht, T. Unold, V. Getautis, S. Albrecht, *Science* **2020**, *370*, 1300.
[27] N.-G. Park, H. Segawa, *ACS Photonics* **2018**, *5*, 2970.
[28] R. Schmager, J. Roger, J. A. Schwenzer, F. Schackmar, T. Abzieher, M. Malekshahi Byranvand, B. Abdollahi Nejand, M. Worgull, B. S. Richards, U. W. Paetzold, *Adv. Energy Mater.* **2020**, *30*, 1907481.
[29] M. Saliba, T. Matsui, K. Domanski, J.-Y. Seo, A. Ummadisingu, S. M. Zakeeruddin, J.-P. Correa-Baena, W. R. Tress, A. Abate, A. Hagfeldt, M. Grätzel, *Science* **2016**, *354*, 206.
[30] M. Saliba, T. Matsui, J.-Y. Seo, K. Domanski, J.-P. Correa-Baena, M. K. Nazeeruddin, S. M. Zakeeruddin, W. Tress, A. Abate, A. Hagfeldt, M. Grätzel, *Energy Environ. Sci.* **2016**, *9*, 1989.
[31] M. M. Lee, J. Teuscher, T. Miyasaka, T. N. Murakami, H. J. Snaith, *Science* **2012**, *338*, 643.
[32] N. K. Noel, S. D. Stranks, A. Abate, C. Wehrenfennig, S. Guarnera, A.-A. Haghighirad, A. Sadhanala, G. E. Eperon, S. K. Pathak, M. B. Johnston, A. Petrozza, L. M. Herz, H. J. Snaith, *Energy Environ. Sci.* **2014**, *7*, 3061.
[33] A. K. Jena, A. Kulkarni, T. Miyasaka, *Chem. Rev.* **2019**, *119*, 3036.
[34] D. P. McMeekin, G. Sadoughi, W. Rehman, G. E. Eperon, M. Saliba, M. T. Hörantner, A. Haghighirad, N. Sakai, L. Korte, B. Rech, M. B. Johnston, L. M. Herz, H. J. Snaith, *Science* **2016**, *351*, 151.
[35] V. M. Goldschmidt, *Naturwissenschaften* **1926**, *14*, 477.
[36] M. Johnsson, P. Lemmens, *J. Phys.: Condens. Matter* **2008**, *20*, 264001.
[37] Z. Li, M. Yang, J.-S. Park, S.-H. Wei, J. J. Berry, K. Zhu, *Chem. Mater.* **2016**, *28*, 284.
[38] F. Ünlü, E. Jung, J. Haddad, A. Kulkarni, S. Öz, H. Choi, T. Fischer, S. Chakraborty, T. Kirchartz, S. Mathur, *APL Mater.* **2020**, *8*, 070901.
[39] G. Kieslich, S. Sun, A. K. Cheetham, *Chem. Sci.* **2015**, *6*, 3430.
[40] R. E. Brandt, V. Stevanović, D. S. Ginley, T. Buonassisi, *MRS Commun.* **2015**, *5*, 265.
[41] T. Umebayashi, K. Asai, T. Kondo, A. Nakao, *Phys. Rev. B* **2003**, *67*, 155405.
[42] J.-W. Lee, S. Tan, S. I. Seok, Y. Yang, N.-G. Park, *Science* **2022**, *375*, eabj1186.
[43] F. Ünlü, E. Jung, S. Öz, H. Choi, T. Fischer, S. Mathur, in *Perovskite Solar Cells: Materials, Processes, and Devices*, Wiley-VCH GmbH, Weinheim, Germany **2021**, p. 1.
[44] L. K. Ono, E. J. Juarez-Perez, Y. Qi, *ACS Appl. Mater. Interfaces* **2017**, *9*, 30197.
[45] N. J. Jeon, J. H. Noh, W. S. Yang, Y. C. Kim, S. Ryu, J. Seo, S. I. Seok, *Nature* **2015**, *517*, 476.
[46] M. Saliba, *Adv. Energy Mater.* **2019**, *9*, 1803754.
[47] A. Hazarika, Q. Zhao, E. A. Gaulding, J. A. Christians, B. Dou, A. R. Marshall, T. Moot, J. J. Berry, J. C. Johnson, J. M. Luther, *ACS Nano* **2018**, *12*, 10327.
[48] L. Protesescu, S. Yakunin, M. I. Bodnarchuk, F. Krieg, R. Caputo, C. H. Hendon, R. X. Yang, A. Walsh, M. V. Kovalenko, *Nano Lett.* **2015**, *15*, 3692.
[49] L. C. Schmidt, A. Pertegás, S. González-Carrero, O. Malinkiewicz, S. Agouram, G. Mínguez Espallargas, H. J. Bolink, R. E. Galian, J. Pérez-Prieto, *J. Am. Chem. Soc.* **2014**, *136*, 850.
[50] J. Shamsi, A. S. Urban, M. Imran, L. De Trizio, L. Manna, *Chem. Rev.* **2019**, *119*, 3296.
[51] X. Li, Y. Wu, S. Zhang, B. Cai, Y. Gu, J. Song, H. Zeng, *Adv. Funct. Mater.* **2016**, *26*, 2435.
[52] F. Zhang, H. Zhong, C. Chen, X.-g. Wu, X. Hu, H. Huang, J. Han, B. Zou, Y. Dong, *ACS Nano* **2015**, *9*, 4533.
[53] A. Swarnkar, R. Chulliyil, V. K. Ravi, M. Irfanullah, A. Chowdhury, A. Nag, *Angew. Chem., Int. Ed.* **2015**, *54*, 15424.
[54] W. Lin, X. Hu, L. Mo, X. Jiang, X. Xing, L. Shui, S. Priya, K. Wang, G. Zhou, *Adv. Opt. Mater.* **2021**, *9*, 2100261.
[55] C. Otero-Martínez, D. García-Lojo, I. Pastoriza-Santos, J. Pérez-Juste, L. Polavarapu, *Angew. Chem., Int. Ed.* **2021**, *60*, 26677.
[56] J. Navarro-Arenas, I. Suárez, A. F. Gualdrón-Reyes, I. Mora-Seró, J. Bisquert, J. P. Martínez-Pastor, *Adv. Opt. Mater.* **2021**, *9*, 2100807.
[57] X. Zhou, J. Zhang, X. Tong, Y. Sun, H. Zhang, Y. Min, Y. Qian, *Adv. Opt. Mater.* **2022**, *10*, 2101517.
[58] J. Y. Lee, S. Y. Kim, H. J. Yoon, *Adv. Opt. Mater.* **2022**, *10*, 2101361.
[59] L. Protesescu, S. Yakunin, S. Kumar, J. Bär, F. Bertolotti, N. Masciocchi, A. Guagliardi, M. Grotevent, I. Shorubalko, M. I. Bodnarchuk, C.-J. Shih, M. V. Kovalenko, *ACS Nano* **2017**, *11*, 3119.
[60] J. A. Vigil, A. Hazarika, J. M. Luther, M. F. Toney, *ACS Energy Lett.* **2020**, *5*, 2475.
[61] M. Hao, Y. Bai, S. Zeiske, L. Ren, J. Liu, Y. Yuan, N. Zarrabi, N. Cheng, M. Ghasemi, P. Chen, M. Lyu, D. He, J.-H. Yun, Y. Du, Y. Wang, S. Ding, A. Armin, P. Meredith, G. Liu, H.-M. Cheng, L. Wang, *Nat. Energy* **2020**, *5*, 79.
[62] J. Yuan, A. Hazarika, Q. Zhao, X. Ling, T. Moot, W. Ma, J. M. Luther, *Joule* **2020**, *4*, 1160.
[63] Q. A. Akkerman, V. D'Innocenzo, S. Accornero, A. Scarpellini, A. Petrozza, M. Prato, L. Manna, *J. Am. Chem. Soc.* **2015**, *137*, 10276.
[64] G. Han, H. D. Hadi, A. Bruno, S. A. Kulkarni, T. M. Koh, L. H. Wong, C. Soci, N. Mathews, S. Zhang, S. G. Mhaisalkar, *J. Phys. Chem. C* **2018**, *122*, 13884.
[65] Y. Fan, H. Meng, L. Wang, S. Pang, *Sol. RRL*, **2019**, *3*, 1900215.
[66] J. H. Heo, S. H. Im, J. H. Noh, T. N. Mandal, C.-S. Lim, J. A. Chang, Y. H. Lee, H.-j. Kim, A. Sarkar, M. K. Nazeeruddin, M. Grätzel, S. I. Seok, *Nat. Photonics* **2013**, *7*, 486.
[67] J. Seo, S. Park, Y. Chan Kim, N. J. Jeon, J. H. Noh, S. C. Yoon, S. I. Seok, *Energy Environ. Sci.* **2014**, *7*, 2642.
[68] N. J. Jeon, J. H. Noh, Y. C. Kim, W. S. Yang, S. Ryu, S. I. Seok, *Nat. Mater.* **2014**, *13*, 897.
[69] W. S. Yang, J. H. Noh, N. J. Jeon, Y. C. Kim, S. Ryu, J. Seo, S. I. Seok, *Science* **2015**, *348*, 1234.
[70] W. S. Yang, B.-W. Park, E. H. Jung, N. J. Jeon, Y. C. Kim, D. U. Lee, S. S. Shin, J. Seo, E. K. Kim, J. H. Noh, S. I. Seok, *Science* **2017**, *356*, 1376.
[71] N. J. Jeon, H. Na, E. H. Jung, T.-Y. Yang, Y. G. Lee, G. Kim, H.-W. Shin, S. Il Seok, J. Lee, J. Seo, *Nat. Energy* **2018**, *3*, 682.
[72] Q. Jiang, Y. Zhao, X. Zhang, X. Yang, Y. Chen, Z. Chu, Q. Ye, X. Li, Z. Yin, J. You, *Nat. Photonics* **2019**, *13*, 460.
[73] G. Kim, H. Min, K. S. Lee, D. Y. Lee, S. M. Yoon, S. I. Seok, *Science* **2020**, *370*, 108.
[74] M. Kim, J. Jeong, H. Lu, T. K. Lee, F. T. Eickemeyer, Y. Liu, I. W. Choi, S. J. Choi, Y. Jo, H.-B. Kim, S.-I. Mo, Y.-K. Kim, H. Lee, N. G. An, S. Cho, W. R. Tress, S. M. Zakeeruddin, A. Hagfeldt, J. Y. Kim, M. Grätzel, D. S. Kim, *Science* **2022**, *375*, 302.
[75] J. Y. Kim, J.-W. Lee, H. S. Jung, H. Shin, N.-G. Park, *Chem. Rev.* **2020**, *120*, 7867.
[76] S. Peng, Z. Wen, T. Ye, X. Xiao, K. Wang, J. Xia, J. Sun, T. Zhang, G. Mei, H. Liu, B. Xu, X. Li, R. Chen, G. Xing, K. Wang, Z. Tang, *ACS Appl. Mater. Interfaces* **2020**, *12*, 31863.

[77] Z. Liu, L. Krückemeier, B. Krogmeier, B. Klingebiel, J. A. Márquez, S. Levcenko, S. Öz, S. Mathur, U. Rau, T. Unold, T. Kirchartz, *ACS Energy Lett.* **2019**, *4*, 110.
[78] C. C. Boyd, R. Cheacharoen, T. Leijtens, M. D. McGehee, *Chem. Rev.* **2019**, *119*, 3418.
[79] M. V. Khenkin, E. A. Katz, A. Abate, G. Bardizza, J. J. Berry, C. Brabec, F. Brunetti, V. Bulović, Q. Burlingame, A. Di Carlo, R. Cheacharoen, Y.-B. Cheng, A. Colsmann, S. Cros, K. Domanski, M. Dusza, C. J. Fell, S. R. Forrest, Y. Galagan, D. Di Girolamo, M. Grätzel, A. Hagfeldt, E. von Hauff, H. Hoppe, J. Kettle, H. Köbler, M. S. Leite, S. Liu, Y.-L. Loo, J. M. Luther, et al., *Nat. Energy* **2020**, *5*, 35.
[80] G. E. Eperon, S. D. Stranks, C. Menelaou, M. B. Johnston, L. M. Herz, H. J. Snaith, *Energy Environ. Sci.* **2014**, *7*, 982.
[81] J. A. Steele, H. Jin, I. Dovgaliuk, R. F. Berger, T. Braeckevelt, H. Yuan, C. Martin, E. Solano, K. Lejaeghere, S. M. J. Rogge, C. Notebaert, W. Vandezande, K. P. F. Janssen, B. Goderis, E. Debroye, Y.-K. Wang, Y. Dong, D. Ma, M. Saidaminov, H. Tan, Z. Lu, V. Dyadkin, D. Chernyshov, V. V. Speybroeck, E. H. Sargent, J. Hofkens, M. B. J. Roeffaers, *Science* **2019**, *365*, 679.
[82] Y. An, J. Hidalgo, C. A. R. Perini, A.-F. Castro-Méndez, J. N. Vagott, K. Bairley, S. Wang, X. Li, J.-P. Correa-Baena, *ACS Energy Lett.* **2021**, *6*, 1942.
[83] A. Marronnier, G. Roma, S. Boyer-Richard, L. Pedesseau, J.-M. Jancu, Y. Bonnassieux, C. Katan, C. C. Stoumpos, M. G. Kanatzidis, J. Even, *ACS Nano* **2018**, *12*, 3477.
[84] C. C. Stoumpos, C. D. Malliakas, M. G. Kanatzidis, *Inorg. Chem.* **2013**, *52*, 9019.
[85] W. Chen, X. Li, Y. Li, Y. Li, *Energy Environ. Sci.* **2020**, *13*, 1971.
[86] A. Khorasani, M. Marandi, R. Khosroshahi, M. Malekshahi Byranvand, M. dehghani, A. Iraji Zad, F. Tajabadi, N. Taghavinia, *ACS Appl. Mater. Interfaces* **2019**, *11*, 30838.
[87] G.-W. Kim, G. Kang, M. Malekshahi Byranvand, G.-Y. Lee, T. Park, *ACS Appl. Mater. Interfaces* **2017**, *9*, 27720.
[88] J. Lee, T. H. Lee, M. M. Byranvand, K. Choi, H. I. Kim, S. A. Park, J. Y. Kim, T. Park, *J. Mater. Chem. A* **2018**, *6*, 5538.
[89] J. Lee, M. Malekshahi Byranvand, G. Kang, S. Y. Son, S. Song, G.-W. Kim, T. Park, *J. Am. Chem. Soc.* **2017**, *139*, 12175.
[90] J.-W. Lee, D.-H. Kim, H.-S. Kim, S.-W. Seo, S. M. Cho, N.-G. Park, *Adv. Energy Mater.* **2015**, *5*, 1501310.
[91] M. Malekshahi Byranvand, F. Behboodi-Sadabad, A. Alrhman Eliwi, V. Trouillet, A. Welle, S. Ternes, I. M. Hossain, M. R. Khan, J. A. Schwenzer, A. Farooq, B. S. Richards, J. Lahann, U. W. Paetzold, *J. Mater. Chem. A* **2020**, *8*, 20122.
[92] N. Pellet, P. Gao, G. Gregori, T.-Y. Yang, M. K. Nazeeruddin, J. Maier, M. Grätzel, *Angew. Chem., Int. Ed.* **2014**, *53*, 3151.
[93] D. Bi, W. Tress, M. I. Dar, P. Gao, J. Luo, C. Renevier, K. Schenk, A. Abate, F. Giordano, J.-P. C. Baena, J.-D. Decoppet, S. M. Zakeeruddin, M. K. Nazeeruddin, M. Grätzel, A. Hagfeldt, *Sci. Adv.* **2016**, *2*, e1501170.
[94] M. Saliba, S. Orlandi, T. Matsui, S. Aghazada, M. Cavazzini, J.-P. Correa-Baena, P. Gao, R. Scopelliti, E. Mosconi, K.-H. Dahmen, F. De Angelis, A. Abate, A. Hagfeldt, G. Pozzi, M. Graetzel, M. K. Nazeeruddin, *Nat. Energy* **2016**, *1*, 15017.
[95] Y. Zhang, G. Grancini, Y. Feng, A. M. Asiri, M. K. Nazeeruddin, *ACS Energy Lett.* **2017**, *2*, 802.
[96] W. Li, A. Thirumurugan, P. T. Barton, Z. Lin, S. Henke, H. H. M. Yeung, M. T. Wharmby, E. G. Bithell, C. J. Howard, A. K. Cheetham, *J. Am. Chem. Soc.* **2014**, *136*, 7801.
[97] A. Binek, F. C. Hanusch, P. Docampo, T. Bein, *J. Phys. Chem. Lett.* **2015**, *6*, 1249.
[98] B. Conings, J. Drijkoningen, N. Gauquelin, A. Babayigit, J. D'Haen, L. D'Olieslaeger, A. Ethirajan, J. Verbeeck, J. Manca, E. Mosconi, F. D. Angelis, H.-G. Boyen, *Adv. Energy Mater.* **2015**, *5*, 1500477.
[99] M. Kulbak, D. Cahen, G. Hodes, *J. Phys. Chem. Lett.* **2015**, *6*, 2452.
[100] T. Duong, H. K. Mulmudi, H. Shen, Y. Wu, C. Barugkin, Y. O. Mayon, H. T. Nguyen, D. Macdonald, J. Peng, M. Lockrey, W. Li, Y.-B. Cheng, T. P. White, K. Weber, K. Catchpole, *Nano Energy* **2016**, *30*, 330.
[101] Y. H. Park, I. Jeong, S. Bae, H. J. Son, P. Lee, J. Lee, C.-H. Lee, M. J. Ko, *Adv. Energy Mater.* **2017**, *27*, 1605988.
[102] N. De Marco, H. Zhou, Q. Chen, P. Sun, Z. Liu, L. Meng, E.-P. Yao, Y. Liu, A. Schiffer, Y. Yang, *Nano Lett.* **2016**, *16*, 1009.
[103] A. D. Jodlowski, C. Roldán-Carmona, G. Grancini, M. Salado, M. Ralaiarisoa, S. Ahmad, N. Koch, L. Camacho, G. de Miguel, M. K. Nazeeruddin, *Nat. Energy* **2017**, *2*, 972.
[104] M. Szafrański, *Thermochim. Acta* **1997**, *307*, 177.
[105] M. Szafrański, A. Katrusiak, *Phys. Rev. B* **2000**, *61*, 1026.
[106] G. Kim, H. Min, S. Lee Kyoung, Y. Lee Do, M. Yoon So, I. Seok Sang, *Science* **2020**, *370*, 108.
[107] H. Lu, Y. Liu, P. Ahlawat, A. Mishra, W. R. Tress, F. T. Eickemeyer, Y. Yang, F. Fu, Z. Wang, C. E. Avalos, B. I. Carlsen, A. Agarwalla, X. Zhang, X. Li, Y. Zhan, S. M. Zakeeruddin, L. Emsley, U. Rothlisberger, L. Zheng, A. Hagfeldt, M. Grätzel, *Science* **2020**, *370*, eabb8985.
[108] T. Singh, T. Miyasaka, *Adv. Energy Mater.* **2018**, *8*, 1700677.
[109] S.-H. Turren-Cruz, A. Hagfeldt, M. Saliba, *Science* **2018**, *362*, 449.
[110] M. M. Byranvand, M. Saliba, *Sol. RRL* **2021**, *5*, 2100295.
[111] M. Abdi-Jalebi, Z. Andaji-Garmaroudi, S. Cacovich, C. Stavrakas, B. Philippe, J. M. Richter, M. Alsari, E. P. Booker, E. M. Hutter, A. J. Pearson, S. Lilliu, T. J. Savenije, H. Rensmo, G. Divitini, C. Ducati, R. H. Friend, S. D. Stranks, *Nature* **2018**, *555*, 497.
[112] T. Bu, X. Liu, Y. Zhou, J. Yi, X. Huang, L. Luo, J. Xiao, Z. Ku, Y. Peng, F. Huang, Y.-B. Cheng, J. Zhong, *Energy Environ. Sci.* **2017**, *10*, 2509.
[113] D. J. Kubicki, D. Prochowicz, A. Hofstetter, S. M. Zakeeruddin, M. Grätzel, L. Emsley, *J. Am. Chem. Soc.* **2018**, *140*, 7232.
[114] S. Wu, Z. Li, J. Zhang, T. Liu, Z. Zhu, A. K. Y. Jen, *Chem. Commun.* **2019**, *55*, 4315.
[115] W. Zhang, J. Xiong, J. Li, W. A. Daoud, *J. Mater. Chem. A* **2019**, *7*, 9486.
[116] E. Jung, K. Budzinauskas, S. Öz, F. Ünlü, H. Kuhn, J. Wagner, D. Grabowski, B. Klingebiel, M. Cherasse, J. Dong, P. Aversa, P. Vivo, T. Kirchartz, T. Miyasaka, P. H. M. van Loosdrecht, L. Perfetti, S. Mathur, *ACS Energy Lett.* **2020**, *5*, 785.
[117] A. Y. Alsalloum, B. Turedi, X. Zheng, S. Mitra, A. A. Zhumekenov, K. J. Lee, P. Maity, I. Gereige, A. AlSaggaf, I. S. Roqan, O. F. Mohammed, O. M. Bakr, *ACS Energy Lett.* **2020**, *5*, 657.
[118] Y. H. Park, I. Jeong, S. Bae, H. J. Son, P. Lee, J. Lee, C.-H. Lee, M. J. Ko, *Adv. Energy Lett.* **2017**, *27*, 1605988.
[119] J.-W. Lee, D.-H. Kim, H.-S. Kim, S.-W. Seo, S. M. Cho, N.-G. Park, *Adv. Energy Lett.* **2015**, *5*, 1501310.
[120] S.-H. Turren-Cruz, A. Hagfeldt, M. Saliba, *Science* **2018**, *362*, 449.
[121] M. Saliba, T. Matsui, K. Domanski, J.-Y. Seo, A. Ummadisingu, S. M. Zakeeruddin, J.-P. Correa-Baena, W. R. Tress, A. Abate, A. Hagfeldt, M. Grätzel, *Science* **2016**, *354*, 206.
[122] G. E. Eperon, T. Leijtens, K. A. Bush, R. Prasanna, T. Green, J. T.-W. Wang, D. P. McMeekin, G. Volonakis, R. L. Milot, R. May, A. Palmstrom, D. J. Slotcavage, R. A. Belisle, J. B. Patel, E. S. Parrott, R. J. Sutton, W. Ma, F. Moghadam, B. Conings, A. Babayigit, H.-G. Boyen, S. Bent, F. Giustino, L. M. Herz, M. B. Johnston, M. D. McGehee, H. J. Snaith, *Science* **2016**, *354*, 861.
[123] T. Chen, B. J. Foley, C. Park, C. M. Brown, L. W. Harriger, J. Lee, J. Ruff, M. Yoon, J. J. Choi, S.-H. Lee, *Sci. Adv.* **2016**, *2*, e1601650.
[124] T. A. S. Doherty, S. Nagane, D. J. Kubicki, Y.-K. Jung, D. N. Johnstone, A. N. Iqbal, D. Guo, K. Frohna, M. Danaie, E. M. Tennyson, S. Macpherson, A. Abfalterer, M. Anaya, Y.-H. Chiang, P. Crout, F. S. Ruggeri, S. Collins, C. P. Grey, A. Walsh, P. A. Midgley, S. D. Stranks, *Science* **2021**, *374*, 1598.

[125] E. M. Mozur, J. R. Neilson, *Annu. Rev. Mater. Res.* **2021**, *51*, 269.
[126] D. H. Fabini, C. C. Stoumpos, G. Laurita, A. Kaltzoglou, A. G. Kontos, P. Falaras, M. G. Kanatzidis, R. Seshadri, *Angew. Chem., Int. Ed.* **2016**, *55*, 15392.
[127] E. M. Mozur, M. A. Hope, J. C. Trowbridge, D. M. Halat, L. L. Daemen, A. E. Maughan, T. R. Prisk, C. P. Grey, J. R. Neilson, *Chem. Mater.* **2020**, *32*, 6266.
[128] A. M. Glazer, *Acta Crystallogr.* **1972**, *28*, 3384.
[129] D. Ghosh, A. R. Smith, A. B. Walker, M. S. Islam, *Chem. Mater.* **2018**, *30*, 5194.
[130] E. M. Mozur, A. E. Maughan, Y. Cheng, A. Huq, N. Jalarvo, L. L. Daemen, J. R. Neilson, *Chem. Mater.* **2017**, *29*, 10168.
[131] E. M. Mozur, J. C. Trowbridge, A. E. Maughan, M. J. Gorman, C. M. Brown, T. R. Prisk, J. R. Neilson, *ACS Mater. Lett.* **2019**, *1*, 260.
[132] P. S. Whitfield, N. Herron, W. E. Guise, K. Page, Y. Q. Cheng, I. Milas, M. K. Crawford, *Sci. Rep.* **2016**, *6*, 35685.
[133] A. J. Knight, J. Borchert, R. D. J. Oliver, J. B. Patel, P. G. Radaelli, H. J. Snaith, M. B. Johnston, L. M. Herz, *ACS Energy Lett.* **2021**, *6*, 799.
[134] A. J. Knight, L. M. Herz, *Energy Environ. Sci.* **2020**, *13*, 2024.
[135] W. Rehman, D. P. McMeekin, J. B. Patel, R. L. Milot, M. B. Johnston, H. J. Snaith, L. M. Herz, *Energy Environ. Sci.* **2017**, *10*, 361.
[136] I. L. Braly, R. J. Stoddard, A. Rajagopal, A. R. Uhl, J. K. Katahara, A. K. Y. Jen, H. W. Hillhouse, *ACS Energy Lett.* **2017**, *2*, 1841.
[137] I. M. Pavlovetc, M. C. Brennan, S. Draguta, A. Ruth, T. Moot, J. A. Christians, K. Aleshire, S. P. Harvey, S. Toso, S. U. Nanayakkara, J. Messinger, J. M. Luther, M. Kuno, *ACS Energy Lett.* **2020**, *5*, 2802.
[138] J.-W. Lee, S.-G. Kim, J.-M. Yang, Y. Yang, N.-G. Park, *APL Mater.* **2019**, *7*, 041111.
[139] L. Liu, J. Lu, H. Wang, Z. Cui, G. Giorgi, Y. Bai, Q. Chen, *Mater. Rep.: Energy* **2021**, *1*, 100064.
[140] K. Domanski, B. Roose, T. Matsui, M. Saliba, S.-H. Turren-Cruz, J.-P. Correa-Baena, C. R. Carmona, G. Richardson, J. M. Foster, F. De Angelis, J. M. Ball, A. Petrozza, N. Mine, M. K. Nazeeruddin, W. Tress, M. Grätzel, U. Steiner, A. Hagfeldt, A. Abate, *Energy Environ. Sci.* **2017**, *10*, 604.
[141] K. C. Kwon, K. Hong, Q. Van Le, S. Y. Lee, J. Choi, K.-B. Kim, S. Y. Kim, H. W. Jang, *Adv. Funct. Mater.* **2016**, *26*, 4213.
[142] Y. Lin, B. Chen, Y. Fang, J. Zhao, C. Bao, Z. Yu, Y. Deng, P. N. Rudd, Y. Yan, Y. Yuan, J. Huang, *Nat. Commun.* **2018**, *9*, 4981.
[143] J. Cao, S. X. Tao, P. A. Bobbert, C.-P. Wong, N. Zhao, *Adv. Mater.* **2018**, *30*, 1707350.
[144] S. van Reenen, M. Kemerink, H. J. Snaith, *J. Phys. Chem. Lett.* **2015**, *6*, 3808.
[145] P. Calado, A. M. Telford, D. Bryant, X. Li, J. Nelson, B. C. O'Regan, P. R. F. Barnes, *Nat. Commun.* **2016**, *7*, 13831.
[146] C. Chen, Z. Song, C. Xiao, R. A. Awni, C. Yao, N. Shrestha, C. Li, S. S. Bista, Y. Zhang, L. Chen, R. J. Ellingson, C.-S. Jiang, M. Al-Jassim, G. Fang, Y. Yan, *ACS Energy Lett.* **2020**, *5*, 2560.
[147] L. T. Schelhas, Z. Li, J. A. Christians, A. Goyal, P. Kairys, S. P. Harvey, D. H. Kim, K. H. Stone, J. M. Luther, K. Zhu, V. Stevanovic, J. J. Berry, *Energy Environ. Sci.* **2019**, *12*, 1341.
[148] N. Li, Y. Luo, Z. Chen, X. Niu, X. Zhang, J. Lu, R. Kumar, J. Jiang, H. Liu, X. Guo, B. Lai, G. Brocks, Q. Chen, S. Tao, D. P. Fenning, H. Zhou, *Joule* **2020**, *4*, 1743.
[149] E. Nakanishi, R. Nishikubo, A. Wakamiya, A. Saeki, *J. Phys. Chem. Lett.* **2020**, *11*, 4043.
[150] D. Ghosh, D. Acharya, L. Zhou, W. Nie, O. V. Prezhdo, S. Tretiak, A. J. Neukirch, *J. Phys. Chem. Lett.* **2019**, *10*, 5000.
[151] S. Feldmann, S. Macpherson, S. P. Senanayak, M. Abdi-Jalebi, J. P. H. Rivett, G. Nan, G. D. Tainter, T. A. S. Doherty, K. Frohna, E. Ringe, R. H. Friend, H. Sirringhaus, M. Saliba, D. Beljonne, S. D. Stranks, F. Deschler, *Nat. Photonics* **2020**, *14*, 123.
[152] J. Chen, M. E. Messing, K. Zheng, T. Pullerits, *J. Am. Chem. Soc.* **2019**, *141*, 3532.
[153] T. Wang, L. Jin, J. Hidalgo, W. Chu, M. Snaider Jordan, S. Deng, T. Zhu, B. Lai, O. Prezhdo, J.-P. Correa-Baena, L. Huang, *Sci. Adv.6*, eabb1336.
[154] T. R. Hopper, A. Gorodetsky, J. M. Frost, C. Müller, R. Lovrincic, A. A. Bakulin, *ACS Energy Lett.* **2018**, *3*, 2199.
[155] Y. Li, T. Ding, X. Luo, Y. Tian, X. Lu, K. Wu, *Chem. Mater.* **2020**, *32*, 549.
[156] M. I. Saidaminov, K. Williams, M. Wei, A. Johnston, R. Quintero-Bermudez, M. Vafaie, J. M. Pina, A. H. Proppe, Y. Hou, G. Walters, S. O. Kelley, W. A. Tisdale, E. H. Sargent, *Nat. Mater.* **2020**, *19*, 412.
[157] L. Liu, J. Lu, H. Wang, Z. Cui, G. Giorgi, Y. Bai, Q. Chen, *Mater. Rep.: Energy* **2021**, *1*, 100064.
[158] A. A. Bakulin, O. Selig, H. J. Bakker, Y. L. A. Rezus, C. Müller, T. Glaser, R. Lovrincic, Z. Sun, Z. Chen, A. Walsh, J. M. Frost, T. L. C. Jansen, *J. Phys. Chem. Lett.* **2015**, *6*, 3663.
[159] O. Selig, A. Sadhanala, C. Müller, R. Lovrincic, Z. Chen, Y. L. A. Rezus, J. M. Frost, T. L. C. Jansen, A. A. Bakulin, *J. Am. Chem. Soc.* **2017**, *139*, 4068.
[160] M. Suri, A. Hazarika, B. W. Larson, Q. Zhao, M. Vallés-Pelarda, T. D. Siegler, M. K. Abney, A. J. Ferguson, B. A. Korgel, J. M. Luther, *ACS Energy Lett.* **2019**, *4*, 1954.
[161] B. Xu, W. Wang, X. Zhang, W. Cao, D. Wu, S. Liu, H. Dai, S. Chen, K. Wang, X. Sun, *J. Mater. Chem. C* **2017**, *5*, 6123.
[162] P. Vashishtha, S. A. Veldhuis, S. S. H. Dintakurti, N. L. Kelly, B. E. Griffith, A. A. M. Brown, M. S. Ansari, A. Bruno, N. Mathews, Y. Fang, T. White, S. G. Mhaisalkar, J. V. Hanna, *J. Mater. Chem. C* **2020**, *8*, 11805.
[163] S. Baek, S. Kim, J. Y. Noh, J. H. Heo, S. H. Im, K.-H. Hong, S.-W. Kim, *Adv. Opt. Mater.* **2018**, *6*, 1800295.
[164] Y. Geng, B. Yang, Y. Xiang, M. Shi, R. Hu, C. Guo, Y. Li, J. Zou, *ChemistrySelect* **2021**, *6*, 8422.
[165] M. T. Hoang, A. S. Pannu, C. Tang, Y. Yang, N. D. Pham, K. Gui, X. Wang, S. Yambem, P. Sonar, A. Du, H. Wang, *Adv. Opt. Mater.* **2020**, *8*, 2000742.
[166] F. Yang, H. Chen, R. Zhang, X. Liu, W. Zhang, J. Zhang, F. Gao, L. Wang, *Adv. Funct. Mater.* **2020**, *30*, 1908760.
[167] T. Binyamin, L. Pedesseau, S. Remennik, A. Sawahreh, J. Even, L. Etgar, *Chem. Mater.* **2020**, *32*, 1467.
[168] S. Li, Z. Shi, F. Zhang, L. Wang, Z. Ma, D. Yang, Z. Yao, D. Wu, T.-T. Xu, Y. Tian, Y. Zhang, C. Shan, X. J. Li, *Chem. Mater.* **2019**, *31*, 3917.
[169] W. Shi, Y. Zhao, C. Xie, P. Yang, *J. Lumin.* **2021**, *233*, 117886.
[170] D. Amgar, T. Binyamin, V. Uvarov, L. Etgar, *Nanoscale* **2018**, *10*, 6060.
[171] G. Mei, Y. Zhang, B. Xu, H. Liu, J. Zhong, K. Shi, X. W. Sun, K. Wang, *J. Phys. D: Appl. Phys.* **2018**, *51*, 454003.
[172] Y.-W. Zhang, G. Wu, H. Dang, K. Ma, S. Chen, *Ind. Eng. Chem. Res.* **2017**, *56*, 10053.
[173] X. Zhang, H. Liu, W. Wang, J. Zhang, B. Xu, K. L. Karen, Y. Zheng, S. Liu, S. Chen, K. Wang, X. W. Sun, *Adv. Mater.* **2017**, *29*, 1606405.
[174] D. Dong, H. Deng, C. Hu, H. Song, K. Qiao, X. Yang, J. Zhang, F. Cai, J. Tang, H. Song, *Nanoscale* **2017**, *9*, 1567.
[175] A. Patra, S. Bera, D. Nasipuri, S. K. Dutta, N. Pradhan, *ACS Energy Lett.* **2021**, *6*, 2682.
[176] M. C. Weidman, M. Seitz, S. D. Stranks, W. A. Tisdale, *ACS Nano* **2016**, *10*, 7830.
[177] J. A. Sichert, Y. Tong, N. Mutz, M. Vollmer, S. Fischer, K. Z. Milowska, R. García Cortadella, B. Nickel, C. Cardenas-Daw, J. K. Stolarczyk, A. S. Urban, J. Feldmann, *Nano Lett.* **2015**, *15*, 6521.

[178] B. Wang, C. Zhang, S. Huang, Z. Li, L. Kong, L. Jin, J. Wang, K. Wu, L. Li, *ACS Appl. Mater. Interfaces* **2018**, *10*, 23303.
[179] H. Wu, Y. Yang, D. Zhou, K. Li, J. Yu, J. Han, Z. Li, Z. Long, J. Ma, J. Qiu, *Nanoscale* **2018**, *10*, 3429.
[180] P. Todorović, D. Ma, B. Chen, R. Quintero-Bermudez, M. I. Saidaminov, Y. Dong, Z.-H. Lu, E. H. Sargent, *Adv. Opt. Mater.* **2019**, *7*, 1901440.
[181] D. Chen, X. Chen, Z. Wan, G. Fang, *ACS Appl. Mater. Interfaces* **2017**, *9*, 20671.
[182] G. Nedelcu, L. Protesescu, S. Yakunin, M. I. Bodnarchuk, M. J. Grotevent, M. V. Kovalenko, *Nano Lett.* **2015**, *15*, 5635.
[183] Y. Liu, G. Pan, R. Wang, H. Shao, H. Wang, W. Xu, H. Cui, H. Song, *Nanoscale* **2018**, *10*, 14067.
[184] P. Todorović, D. Ma, B. Chen, R. Quintero-Bermudez, M. I. Saidaminov, Y. Dong, Z.-H. Lu, E. H. Sargent, **2019**, *7*, 1901440.
[185] G. Getachew, W.-W. Huang, T.-H. Chou, A. S. Rasal, J.-Y. Chang, *J. Colloid Interface Sci.* **2022**, *605*, 500.
[186] F. Meng, X. Liu, X. Cai, Z. Gong, B. Li, W. Xie, M. Li, D. Chen, H.-L. Yip, S.-J. Su, *Nanoscale* **2019**, *11*, 1295.
[187] S. N. Habisreutinger, D. P. McMeekin, H. J. Snaith, R. J. Nicholas, *APL Mater.* **2016**, *4*, 091503.
[188] H. Zhang, X. Ren, X. Chen, J. Mao, J. Cheng, Y. Zhao, Y. Liu, J. Milic, W.-J. Yin, M. Grätzel, W. C. H. Choy, *Energy Environ. Sci.* **2018**, *11*, 2253.
[189] M. Que, Z. Dai, H. Yang, H. Zhu, Y. Zong, W. Que, N. P. Padture, Y. Zhou, O. Chen, *ACS Energy Lett.* **2019**, *4*, 1970.
[190] J. Chen, D. Jia, E. M. J. Johansson, A. Hagfeldt, X. Zhang, *Energy Environ. Sci.* **2021**, *14*, 224.
[191] J. Khan, I. Ullah, J. Yuan, *Mater. Adv.* **2022**, *3*, 1931.
[192] Q. Zhao, A. Hazarika, X. Chen, S. P. Harvey, B. W. Larson, G. R. Teeter, J. Liu, T. Song, C. Xiao, L. Shaw, M. Zhang, G. Li, M. C. Beard, J. M. Luther, *Nat. Commun.* **2019**, *10*, 2842.
[193] V. K. Ravi, A. Swarnkar, R. Chakraborty, A. Nag, *Nanotechnology* **2016**, *27*, 325708.
[194] Q. A. Akkerman, M. Gandini, F. Di Stasio, P. Rastogi, F. Palazon, G. Bertoni, J. M. Ball, M. Prato, A. Petrozza, L. Manna, *Nat. Energy* **2016**, *2*, 16194.
[195] E. M. Sanehira, A. R. Marshall, J. A. Christians, S. P. Harvey, P. N. Ciesielski, L. M. Wheeler, P. Schulz, L. Y. Lin, M. C. Beard, J. M. Luther, *Sci. Adv.* **2017**, *3*, eaao4204.
[196] C. Otero-Martínez, N. Fiuza-Maneiro, L. Polavarapu, *ACS Appl. Mater. Interfaces* **2022**.
[197] F. Li, S. Zhou, J. Yuan, C. Qin, Y. Yang, J. Shi, X. Ling, Y. Li, W. Ma, *ACS Energy Lett.* **2019**, *4*, 2571.
[198] L. Xie, P. Vashishtha, T. M. Koh, P. C. Harikesh, N. F. Jamaludin, A. Bruno, T. J. N. Hooper, J. Li, Y. F. Ng, S. G. Mhaisalkar, N. Mathews, *Adv. Mater.* **2020**, *32*, 2003296.
[199] S. Y. Park, H. C. Shim, *ACS Appl. Mater. Interfaces* **2020**, *12*, 57124.
[200] X.-K. Liu, W. Xu, S. Bai, Y. Jin, J. Wang, R. H. Friend, F. Gao, *Nat. Mater.* **2021**, *20*, 10.
[201] G. Pacchioni, *Nat. Rev. Mater.* **2021**, *6*, 108.
[202] Q. Van Le, H. W. Jang, S. Y. Kim, *Small Methods* **2018**, *2*, 1700419.
[203] C. Otero-Martínez, J. Ye, J. Sung, I. Pastoriza-Santos, J. Pérez-Juste, Z. Xia, A. Rao, R. L. Z. Hoye, L. Polavarapu, *Adv. Mater.* **2021**, 10, 2107105.
[204] H. Cho, J. S. Kim, C. Wolf, Y.-H. Kim, H. J. Yun, S.-H. Jeong, A. Sadhanala, V. Venugopalan, J. W. Choi, C.-L. Lee, R. H. Friend, T.-W. Lee, *ACS Nano* **2018**, *12*, 2883.
[205] X. Guo, I. M. Asuo, A. Pignolet, R. Nechache, S. G. Cloutier, *Opt. Mater. Express* **2022**, *12*, 153.
[206] F. Liu, X. Qin, B. Han, C. C. S. Chan, C. Ma, T. L. Leung, W. Chen, Y. He, I. Lončarić, L. Grisanti, J. Ovčar, Ž. Skoko, Y. Shi, F. C. C. Ling, M. R. Huqe, J. A. Zapien, S. Wang, C.-J. Su, U. S. Jeng, K. S. Wong, A. M. C. Ng, M. Gu, J. Popović, A. B. Djurišić, *Adv. Opt. Mater.* **2021**, *9*, 2100393.
[207] G. Xie, C. Jiang, J. Wang, C. Mai, G. Huang, Y. Ma, J. Wang, J. Peng, Y. Cao, *Org. Electron.* **2019**, *71*, 58.
[208] J. Wang, C. Song, Z. He, C. Mai, G. Xie, L. Mu, Y. Cun, J. Li, J. Wang, J. Peng, Y. Cao, *Adv. Mater.* **2018**, *30*, 1804137.
[209] M. Ban, Y. Zou, J. P. H. Rivett, Y. Yang, T. H. Thomas, Y. Tan, T. Song, X. Gao, D. Credgington, F. Deschler, H. Sirringhaus, B. Sun, *Nat. Commun.* **2018**, *9*, 3892.
[210] S. Zhang, H. Liu, X. Li, S. Wang, *Nano Energy* **2020**, *77*, 105302.
[211] K. Sivalertporn, L. Mouchliadis, A. L. Ivanov, R. Philp, E. A. Muljarov, *Phys. Rev. B* **2012**, *85*, 045207.
[212] A. Kanwat, E. Moyen, S. Cho, J. Jang, *ACS Appl. Mater. Interfaces* **2018**, *10*, 16852.
[213] Y. Shi, J. Xi, T. Lei, F. Yuan, J. Dai, C. Ran, H. Dong, B. Jiao, X. Hou, Z. Wu, *ACS Appl. Mater. Interfaces* **2018**, *10*, 9849.
[214] Z. Xiao, Q. Wang, X. Wu, Y. Wu, J. Ren, Z. Xiong, X. Yang, *Org. Electron.* **2020**, *77*, 105546.
[215] F. Zhang, J. Song, B. Cai, X. Chen, C. Wei, T. Fang, H. Zeng, *Sci. Bull.* **2021**, *66*, 2189.
[216] L. Zhang, C. Sun, T. He, Y. Jiang, J. Wei, Y. Huang, M. Yuan, *Light: Sci. Appl.* **2021**, *10*, 61.
[217] G. S. Kumar, R. R. Sumukam, B. Murali, *J. Mater. Chem. C* **2020**, *8*, 14334.
[218] M. Ren, S. Cao, J. Zhao, B. Zou, R. Zeng, *Nano-Micro Lett.* **2021**, *13*, 163.
[219] M. Karlsson, Z. Yi, S. Reichert, X. Luo, W. Lin, Z. Zhang, C. Bao, R. Zhang, S. Bai, G. Zheng, P. Teng, L. Duan, Y. Lu, K. Zheng, T. Pullerits, C. Deibel, W. Xu, R. Friend, F. Gao, *Nat. Commun.* **2021**, *12*, 361.
[220] A. R. B. M. Yusoff, A. E. X. Gavim, A. G. Macedo, W. J. da Silva, F. K. Schneider, M. A. M. Teridi, *Mater. Today Chem.* **2018**, *10*, 104.
[221] Q. Tao, P. Xu, M. Li, W. Lu, *npj Comput. Mater.* **2021**, *7*, 23.
[222] M. Srivastava, J. M. Howard, T. Gong, M. Rebello Sousa Dias, M. S. Leite, *J. Phys. Chem. Lett.* **2021**, *12*, 7866.
[223] L. E. Mundt, L. T. Schelhas, *Adv. Energy Mater.* **2020**, *10*, 1903074.
[224] L. Gil-Escrig, C. Dreessen, F. Palazon, Z. Hawash, E. Moons, S. Albrecht, M. Sessolo, H. J. Bolink, *ACS Energy Lett.* **2021**, *6*, 827.
[225] J. Yang, Q. Hong, Z. Yuan, R. Xu, X. Guo, S. Xiong, X. Liu, S. Braun, Y. Li, J. Tang, C. Duan, M. Fahlman, Q. Bao, *Adv. Opt. Mater.* **2018**, *6*, 1800262.
[226] M. Alsari, O. Bikondoa, J. Bishop, M. Abdi-Jalebi, L. Y. Ozer, M. Hampton, P. Thompson, M. T. Hörantner, S. Mahesh, C. Greenland, J. E. Macdonald, G. Palmisano, H. J. Snaith, D. G. Lidzey, S. D. Stranks, R. H. Friend, S. Lilliu, *Energy Environ. Sci.* **2018**, *11*, 383.
[227] F. Babbe, C. M. Sutter-Fella, *Adv. Energy Mater.* **2020**, *10*, 1903587.

Mahdi Malekshahi Byranvand is a researcher at the Forschungszentrum Jülich and Institute for Photovoltaics (ipv) at the University of Stuttgart. Previously, he worked on different parts of perovskite solar cells during his postdoctoral fellows at Karlsruhe Institute of Technology (KIT), Pohang University of Science and Technology (POSTECH), and Sharif University of technology. He received his Ph.D. inorganic chemistry at the University of Tehran in 2015, working on photon management in dye-sensitized solar cells. His research interests are currently focused on passivation techniques of perovskite films and perovskite-silicon tandem solar cells in the Prof. Michael Saliba group.

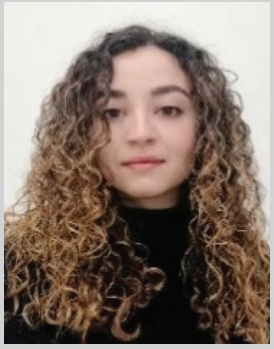

Clara Otero received her master's degree in chemical research and industrial chemistry from the University of Vigo in 2020. Now, she is a Ph.D. candidate in the Materials Chemistry and Physics group with Dr. Lakshminarayana Polavarapu. Her research interests are focused on the synthesis and study of the optical properties of hybrid and inorganic halides perovskites, and their optoelectronic applications.

Junzhi Ye received his bachelor's degree in chemical and materials engineering at the University of Auckland, New Zealand. He is currently a Ph.D. student in Cavendish Laboratory, Department of Physics at the University of Cambridge (2019–). His primary supervisor is Dr. Akshay Rao and co-supervised by Dr. Robert Hoye. His research interests are currently focused on perovskite optoelectronic devices, including perovskite quantum dots light-emitting diodes and perovskite-silicon tandem solar cells.

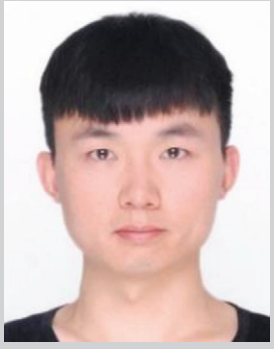

Weiwei Zuo is a Ph.D. student in the Institute for Photovoltaics (ipv) at the University of Stuttgart, Germany, under the supervision of Prof. Michael Saliba since 2019. He graduated from Zhengzhou University in China and worked on optoelectronic functional materials and fabrication of optoelectronic devices, involving 2D materials, synthesis of optoelectronic organic small molecules, and fabrication of OLED and OPV devices. From 2017 to 2019, he was a visiting student under the supervision of Prof. Antonio Abate in HZB and focused on the fabrication of perovskite solar cells. His current research interests are the crystallization and device physics of perovskite solar cells.

Liberato Manna obtained his Bachelor's Degree in Chemistry in 1996 from the University of Bari and Ph.D. in Chemistry in 2001 from the same University, and worked at UC Berkeley (USA) as a visiting Student (1999–2000) and subsequently at the Lawrence Berkeley Lab (USA) as a postdoctoral fellow (2001–2003). He then started his career as independent PI at the National Nanotechnology Lab in Lecce (Italy, 2003–2009) and later moved to the Istituto Italiano di Tecnologia (IIT), Genova (Italy) as head of the Nanochemistry Group. Since 2016 he has regularly taught at the University of Genova. Since 2015 he is also associate director of IIT for the Materials and Nanotechnology programs. His research interests include the synthesis and assembly of colloidal nanocrystals, the structural, chemical, and surface transformations in nanoscale materials, and their applications in energy, photonics, and electronics.

Michael Saliba is the director of the Institute for Photovoltaics (ipv) at the University of Stuttgart with a dual appointment as the Helmholtz Young Investigator at the Forschungszentrum Jülich, Germany. His research focuses on a deeper fundamental understanding and improvement of optoelectronic properties of emerging photovoltaic materials with an emphasis on perovskites for a sustainable energy future. Previously, he held positions at TU Darmstadt, University of Fribourg, and EPFL. He obtained his Ph.D. at Oxford University. Among others, he received the Heinz-Maier-Leibnitz Award of the German Research Foundation and was named as one of the world-wide 35 innovators under 35 by the MIT Technology Review.

Robert Hoye is a Lecturer (Assistant Professor) in the Department of Materials at Imperial College London. There, he also holds a Royal Academy of Engineering Research Fellowship. He completed his Ph.D. at the University of Cambridge (2012–2014), before working as a postdoctoral researcher at the Massachusetts Institute of Technology (2015–2016). He subsequently received two College Research Fellowships at Cambridge, firstly at Magdalene College (2016–2019), then at Downing College (2019–2020), before taking up his Lectureship at Imperial in 2020. His research focuses on defect-tolerant semiconductors, and their development into optoelectronic devices

Lakshminarayana Polavarapu is the principal investigator of the Materials chemistry and physics research group at the Centro De Investigaciones Biomédicas (CINBIO), University of Vigo. He obtained an MSc in Chemistry from the University of Hyderabad (India) and Ph.D. from the National University of Singapore. After being a postdoctoral fellow at CIC biomaGUNE and University of Vigo in Spain, he joined the Chair for Photonics and Optoelectronics at the Ludwig-Maximilians-University of Munich (Germany) as an Alexander von Humboldt postdoctoral fellow and later continued as a junior group leader until May 2020. His research interests include shape-controlled synthesis and self-assembly of metal and semiconductor nanocrystals for exploring their optical properties and optoelectronic applications.